Multi-model assessment of the factors driving stratospheric ozone evolution over the 21st century

L. D. Oman[1,2], D. A. Plummer[3], D. W. Waugh[2], J. Austin[4], J. Scinocca[3], A. R. Douglass[1], R. J. Salawitch[5], T. Canty[5], H. Akiyoshi[6], S. Bekki[7], P. Braesicke[8], N. Butchart[9], M. P. Chipperfield[10], D. Cugnet[7], S. Dhomse[10], V. Eyring[11], S. Frith[1,12], S. C. Hardiman[9], D. E. Kinnison[13], J. F. Lamarque[13], E. Mancini[14], M. Marchand[7], M. Michou[15], O. Morgenstern[16], T. Nakamura[6], J. E. Nielsen[1,12], D. Olivié[15], G. Pitari[14], J. Pyle[8], E. Rozanov[17], T. G. Shepherd[18], K. Shibata[19], R. S. Stolarski[1], H. Teyssèdre[15], W. Tian[10], Y. Yamashita[6]

[1] NASA Goddard Space Flight Center, Greenbelt, Maryland
[2] Department of Earth and Planetary Sciences, Johns Hopkins University, Baltimore, Maryland
[3] Canadian Centre for Climate Modelling and Analysis, Victoria, BC, Canada
[4] NOAA Geophysical Fluid Dynamics Laboratory, Princeton, New Jersey
[5] University of Maryland, College Park, Maryland
[6] NIES, Tsukuba, Japan.
[7] IPSL, France.
[8] University of Cambridge, UK.
[9] Met. Office, UK.
[10] University of Leeds, UK.
[11] Deutsches Zentrum für Luft- und Raumfahrt, Institut für Physik der Atmosphäre, Oberpfaffenhofen, Germany.
[12] Science Systems and Applications, Inc. (SSAI), Beltsville, MD.
[13] NCAR, Boulder CO.
[14] University of L'Aquila, Italy.
[15] GAME/CNRM (Météo-France, CNRS), France.
[16] National Institute of Water and Atmospheric Research, Lauder, NZ.
[17] PMOD/WRC and IAC ETHZ, Switzerland.
[18] University of Toronto, Toronto, Ontario, Canada.
[19] MRI, Japan.

To be submitted to JGR-Atmospheres
Draft as of April 2010

Corresponding Author:
Luke D. Oman
NASA Goddard Space Flight Center
Atmospheric Chemistry and Dynamics Branch
Code 613.3
Greenbelt, MD 20771
E-mail: luke.d.oman@nasa.gov

Abstract

The evolution of stratospheric ozone from 1960 to 2100 is examined in simulations from fourteen chemistry-climate models. There is general agreement among the models at the broadest levels, showing column ozone decreasing at all latitudes from 1960 to around 2000, then increasing at all latitudes over the first half of the 21st century, and latitudinal variations in the rate of increase and date of return to historical values. In the second half of the century, ozone is projected to continue increasing, level off or even decrease depending on the latitude, resulting in variable dates of return to historical values at latitudes where column ozone has declined below those levels. Separation into partial column above and below 20 hPa reveals that these latitudinal differences are almost completely due to differences in the lower stratosphere. At all latitudes, upper stratospheric ozone increases throughout the 21st century and returns to 1960 levels before the end of the century, although there is a spread among the models in dates that ozone returns to historical values. Using multiple linear regression, we find decreasing halogens and increasing greenhouse gases contribute almost equally to increases in the upper stratospheric ozone. In the tropical lower stratosphere an increase in tropical upwelling causes a steady decrease in ozone through the 21st century, and total column ozone does not return to 1960 levels in all models. In contrast, lower stratospheric and total column ozone in middle and high latitudes increases during the 21st century and returns to 1960 levels.

1. Introduction

The evolution of ozone in the 21st century is a critical science issue. While changes in ozone are presently controlled primarily by declines in halogen concentrations, variations in temperature, circulation, and oxides of nitrogen and hydrogen also affect ozone [*WMO* 2003; *WMO* 2007]. Throughout the stratosphere there are long-term changes in various processes and the balances among them. Therefore it is difficult to find a single approach to identify the contributions of different mechanisms affecting ozone levels throughout the stratosphere.

Ozone loss throughout much of the stratosphere was dominated by rising halogen concentrations until about 1997, the time of peak halogen loading [e.g., *Yang et al.*, 2006; *Shepherd and Jonsson*, 2008; *Yang et al.*, 2008]. In the 21st century, as halogen concentrations are expected to decrease at about 1/3 of the rate of their increase in the late 20th century, other factors will likely play a more significant role in the evolution of ozone. Stratospheric cooling will decrease the rate of gas-phase reactions that destroy ozone, and thereby increase concentrations of ozone [e.g., *Haigh and Pyle*, 1979; *Brasseur and Hitchman*, 1988; *Shindell et al.*, 1998; *Rosenfield et al.*, 2002]. Future increases in N_2O and CH_4 increase loss of ozone by nitrogen and hydrogen catalytic cycles, [e.g., *Randeniya et al.*, 2002; *Rosenfield et al.*, 2002; *Chipperfield and Feng*, 2003; *Portmann and Solomon*, 2007; *Ravishankara et al.*, 2009] but in a changing climate, increases in N_2O do not necessarily cause NO_y (or NO_x) to increase proportionately throughout the stratosphere. *Rosenfield and Douglass* (1998) showed that NO_y loss rates increase as the stratosphere cools, which will impact future levels of ozone. Several studies have linked increases in greenhouse gases (GHGs) to changes in stratospheric transport,

86 further impacting ozone recovery [*Waugh et al.*, 2009; *Li et al.*, 2009; *Hegglin and Shepherd*,
87 2009].

88 *Eyring et al.* [2005] laid the groundwork for the Chemistry-Climate Model Validation
89 (CCMVal) activity in which numerous chemistry-climate models (CCMs) were evaluated to
90 increase our confidence in predicting future stratospheric ozone change. The results of the
91 CCMVal-1 simulations of past ozone changes conducted for this activity were presented in
92 *Eyring et al.* [2006], which evaluated processes important in determining the distribution of
93 ozone. In a follow on study *Eyring et al.* [2007] presented the projections of stratospheric ozone
94 change over the 21st century simulated by these CCMs, and discussed how quantities that can
95 impact ozone are projected to change.

96 CCMVal-1 was the first major coordinated activity where an ensemble of CCMs
97 performed simulations with similar external forcings to assess ozone evolution [*Eyring et al.*,
98 2007]. The CCMVal-2 activity [*Eyring et al.*, 2008] included more models (14 are used here)
99 and, in addition, more simulations cover the entire period of interest (1960-2100) than in
100 CCMVal-1 (3 models). Here, we make use of CCMs that participated in the CCMVal-2 activity
101 and that contributed projections of stratospheric ozone evolution until the end of the 21st century.
102 These simulations are based on observed GHG and halogen concentrations in the past and on one
103 predicted scenario for the future.

104 *Austin et al.* [2010a] examined the evolution of total column ozone and compared ozone
105 and Cl_y recovery dates in the CCMVal-2 models. Here we (a) contrast the evolution in the upper
106 and lower stratosphere, and (b) examine the causes of the ozone changes (and differences among
107 the models). To accomplish this, we apply a variety of methods depending on the physical
108 and/or chemical processes that dominate ozone evolution in various regions. Section 2 gives an

109 overview of the models and model simulations. The results are discussed for extra-polar ozone
110 in Section 3 and polar ozone in Section 4. Variations in ozone recovery by region are discussed
111 in Section 5 and a summary of the conclusions is given in Section 6.
112
113
114 **2.1 Models and Model Simulations**
115
116 CCMVal-2 model simulations were conducted to improve the understanding of models
117 through process-oriented evaluation along with discussion and coordinated analysis [*SPARC,*
118 2010]. Information about individual model simulations and references for each are summarized
119 in Table 1. In addition, *Morgenstern et al.* [2010] present a much more detailed overview of the
120 models that participated in this activity. Here we consider 1960 to 2100 simulations from the
121 CCMs whose domains include at least the upper stratosphere, and can then be used to contrast
122 the ozone evolution in the lower and upper stratosphere. All models in this study have output for
123 1960-2099, except UMUKCA-METO which ends in 2083.
124 REF-B2 uses the A1b GHG scenario from IPCC [2000] and the adjusted A1 halogen
125 scenario from WMO [2007]. The adjusted A1 halogen scenario includes the earlier phase out of
126 hydrochlorofluorocarbons mandated by recent revisions to the Montreal Protocol. For
127 GEOSCCM a combination of REF-B1 (1960-2000) and REF-B2 (2001-2099) was used. REF-
128 B1 differs only in that observed Hadley sea surface temperatures (SST) and sea ice data [*Rayner*
129 *et al.,* 2003] were used instead of modeled SSTs. All model runs with the exception of CMAM
130 use prescribed sea surface temperatures and sea ice extent based on fully coupled atmosphere-
131 ocean runs for the A1b scenario. CMAM includes a fully coupled ocean model in its

132 simulations. All models use sophisticated stratospheric chemistry schemes except AMTRAC3,
133 in which halogens are not explicitly modeled but rather Cl_y and Br_y are parameterized [*Austin*
134 *and Wilson*, 2010; *Morgenstern et al.*, 2010]. REF-B2 simulations use background non-volcanic
135 aerosol loading and there are no imposed solar cycle variations. Although several modeling
136 groups submitted multiple ensemble simulations, only one member from each group was used in
137 this analysis because the intermodel differences are generally much larger than the ensemble
138 spreads [*Eyring et al.*, 2007]. The model output used in this study is a zonal mean monthly mean
139 average. The partial and total column ozone amounts are integrated over the standard CCMVal-
140 2 pressure levels.

141 In order to view all 14 models on a single plot, filtering is necessary to remove short-term
142 (e.g. high frequency) variations. In all cases (except where noted) a 1:2:1 filter is used iteratively
143 30 times as described in *Eyring et al.* [2007] to smooth the model output displayed in the figures.
144 While some differences can be seen in individual models between this filter and the time series
145 additive-model (TSAM) analysis, they are typically very small and do not impact our
146 conclusions [*Scinocca et al.* 2010, in preparation].

147

148 **2.2 MLR Analysis**

149

150 One of the primary methods we use to estimate the contribution of different mechanisms
151 to the simulated changes in ozone is multiple linear regression (MLR). The method is explained
152 in detail in *Oman et al.* [2010], but we repeat some of the basic details here. For a given location
153 and time, MLR is applied to determine the coefficients m_X such that

154 $$\Delta O_3(t) = \sum_j m_{X_j} \Delta X_j(t) + \varepsilon(t), \quad (1)$$

155 where the X_j are the different quantities that could influence ozone, the coefficients m_X are the
156 sensitivity of ozone to the quantities X, i.e., $m_X = \partial O_3/\partial X$, and ε is the error in the fit. To do
157 this four explanatory variables (X_j) are used in (1): (i) $Cl_y + \alpha Br_y$, (ii) reactive nitrogen (NO_y
158 = $NO+NO_2+NO_3+2*(N_2O_5)+HNO_3+HO_2NO_2+ClONO_2+BrONO_2$), (iii) reactive hydrogen (HO_x
159 = $OH+HO_2$), and (iv) temperature (T). Each term on the right hand side of equation (1) gives the
160 "contribution" of the response in ozone due to a change in X. We use $\alpha = 5$ in the definition as
161 *Daniel et al.* [1999] show this is an appropriate value for the upper stratosphere, which is the
162 chemically driven region for which the MLR analysis is most appropriate. A test of this method
163 using $\alpha = 60$ did not noticeably impact any of the individual contributions calculated in this
164 study. We do use $\alpha = 60$ in section 4 when examining polar lower stratospheric ozone changes.
165 There are several limitations with the above linear regression approach as discussed in
166 Oman et al. [2010] which are summarized below. First, other mechanisms that are not considered
167 in the regression (e.g., transport) could play a role. Second, significant correlations can exist
168 between the temporal variations of the quantities, i.e., the quantities are not necessarily
169 independent. Third, a high correlation between ozone and a quantity does not show causality, as
170 ozone could be causing the quantity to change, or changes in another quantity could be causing
171 both ozone and the quantity of interest to change in a correlated way. Temperature and ozone in
172 the upper stratosphere are an example of this third complication: changes in ozone cause changes
173 in temperature through changes in short-wave heating [*Shepherd and Jonsson*, 2008]. At the
174 same time, the local ozone concentration responds to changes in temperature by changing
175 chemical reaction rates. Also, the relationship between the regression variables and ozone may
176 not be linear. For example, the ClO/Cl_y ratio varies as a function of temperature in a highly non-
177 linear manner. One could use a regression based on the rates of odd-oxygen loss by nitrogen,

178 chlorine, and bromine radical abundances as regressor variables, as was done by *Yang et al.*,
179 [2006]. However, this treatment is beyond the scope of the present analysis, as the information
180 archived by each model makes use of radical abundances challenging. Because of the above
181 limitations, caution must be applied when interpreting the MLR results presented below.

182 UMUKCA-UCAM and AMTRAC3 did not provide HO_x so for these models the MLR
183 consists of three explanatory variables. This analysis has been repeated without HO_x for all
184 models and while there is some decrease in explained variance from the MLR the main findings
185 and conclusions are not impacted.

186

187 **3. Extra-Polar Ozone**

188

189 ***3.1 Total column ozone***

190

191 *Austin et al.* [2010a] examined the changes in total column ozone in the CCMVal-2
192 simulations. Here, we start with total column ozone and then break down the ozone amounts
193 into two partial columns for the extra-polar region. Figure 1a-c shows the evolution of total
194 column ozone amounts over the tropics (25°S-25°N) and midlatitudes of each hemisphere (35-
195 60°S and 35-60°N), for each of the CCMVal-2 models. The evolution is shown with respect to
196 1960 levels, and has been smoothed as described above. Also shown are ground-based total
197 column ozone measurements (solid black curves, updated from *Fioletov et al.*, [2002]) with
198 respect to the smoothed 1964 value.

199 There is qualitative agreement in the evolution of ozone between regions and models at
200 the broadest level, with ozone decreasing from 1960 to around 2000, and then increasing in the

first half of the 21st century [*Austin et al.*, 2010a]. All models consistently indicate tropical total column ozone at the end of the 21st century is less than it was in 1960 (Figure 1b). In contrast, total column ozone over the midlatitudes (Figures 1a,c) in 2100 exceeds 1960 values in nearly all the models, with a generally larger increase in Northern Hemisphere (NH) mid-latitudes.

There is a large spread in the magnitude of the peak ozone loss (around 2000) and the date that column ozone is predicted to return to 1960 levels. For example, in SH mid-latitudes the simulated decrease in ozone from 1960 to 2000 varies from around 10 DU to over 50 DU, while the date of return to 1960 levels for the same region varies from around 2030 to after 2100. In all three latitude bands CNRM-ACM and MRI show the largest loss in total column ozone by the year 2000, and also tend to have later return dates. UMUKCA-METO has the smallest ozone loss in the tropics and Southern Hemisphere (SH), and one of the smallest decreases in NH midlatitudes. The reasons for these model differences are examined in Section 3.2. Also, there is a large difference in the ozone decline in the SH midlatitudes prior to 1975 found by the various models (declines ranging from 0 to 20 DU), with no change over this time period apparent in the ground-based ozone observations. Ground-based total column ozone observations indicate about a 20 DU decrease by 2000 in the SH midlatitudes and about a 15 DU decrease in the NH midlatitudes. In the tropics only small total column ozone changes have been observed and are less than the model-simulated changes with the exception of UMUKCA-METO, which are similar.

3.2 Partial column ozone

While the evolution of total column ozone and its impact on surface UV radiation changes are of great importance, it is useful to look at changes in the partial columns [e.g., *Yang et al.*, 2006; *Li et al.*, 2009]. This shows the relative role of changes in the upper and lower portions of the stratosphere in the differences described above. As in Oman et al. [2010] we split the stratosphere at 20 hPa because the ozone changes at 20 hPa are generally small, and 20 hPa separates the photochemically controlled ozone region above from the transport and chemically driven region below. Other studies have used 15 hPa [e.g. *Li et al.*, 2009] or 25 km altitude (~25 hPa) [e.g., *Yang et al.*, 2006] but we prefer 20 hPa, as used in *Oman et al.*, [2010].

Figures 1d,e,f and 1g,h,i show the evolution of the partial column ozone amounts for the upper (20 to 0.1 hPa) and lower (500 to 20 hPa) portions of the column. The evolution in the upper partial column ozone is similar among the 3 regions, but there are significant differences in the lower partial column. It is the differences in the lower stratosphere that cause differences in the evolution of column ozone between regions. In particular, the decrease in tropical column ozone over the latter half of the 21st century is due to decreases in the lower stratosphere (Figure 1h), which are larger than increases in upper stratospheric ozone (Figure 1e).

There are quantitative differences in the upper columns but these are generally smaller than the differences in the lower columns, especially in midlatitudes (note the different scales for upper and lower column plots in Figure 1). Peak losses occur around the year 2000, averaging 3 to 7 DU over tropical and midlatitudes for the upper partial column of most models, with MRI and CNRM-ACM having losses around 10 DU. In the lower partial column there are much greater differences in the ozone change over this range of latitude bands. Midlatitude ozone losses around 2000 are largest in the SH, as expected due to the effects of the Antarctic ozone hole [*Atkinson et al.*, 1989]. Ozone losses range from 10-25 DU with less ozone loss in

246 UMUKCA-METO and significantly more in MRI and CNRM-ACM. Tropical latitudes show
247 largest loss of ozone by the end of the 21st century, with a range of 7 to 18 DU. The tropical
248 lower partial column is the only region where ozone is consistently forecast to continue to
249 decline until the end of the 21st century, due to increased strength of the Brewer-Dobson
250 circulation in the models that is driven by rising GHG concentrations [*Rind et al.*, 1998; *Buchart*
251 *and Scaife*, 2001; *Butchart et al.*, 2006; *Shepherd*, 2008; *Li et al.*, 2009]. It should be noted that
252 models with larger (smaller) total column ozone changes generally have larger (smaller) changes
253 in both lower and upper partial columns.
254
255 ***3.3 Upper Stratosphere***
256
257 As discussed above, and shown in Figure 1d-f, the evolution of ozone in the upper portion of the
258 stratosphere is qualitatively similar among most models. Also, the overall behavior of ozone in
259 the tropics and midlatitudes (both hemisphere) is similar. Nonetheless, there are quantitative
260 differences among the models. We use the MLR analysis described in Section 2 to examine the
261 mechanisms causing the ozone changes, and the differences among the models.
262 We consider first the evolution of ozone at 5 hPa in the tropics (25°S-25°N). Figure 2a
263 shows the evolution of the ozone mixing ratio while Figure 2b shows the change in ozone with
264 respect to 1960 levels. There is a large spread in the time-mean values of ozone among the
265 models (from around 8 ppmv to around 11 ppmv), and also some differences in changes relative
266 to 1960 levels. All models show a peak ozone loss around 2000, with magnitudes of 0.5 and 0.7
267 ppm for most models. The MRI and CNRM-ACM models show the largest peak ozone loss
268 (greater than 1.0 ppm), whereas AMTRAC3 and LMDZrepro have the smallest loss (less than

269 0.4 ppm). All models also show 5 hPa ozone returning to 1960 levels before the end of the 21st
270 century, but there is a large spread in dates when this occurs (from early 2020s to 2060s).

271 As presented in the Introduction, several mechanisms can cause changes in ozone,
272 including changes in halogens, temperature, reactive nitrogen and hydrogen, and transport.
273 Figures 2c,e,g,i show the evolution of $Cl_y+\alpha Br_y$, temperature, NO_y, and HO_x, respectively. The
274 evolution of $Cl_y+\alpha Br_y$ and variation among models (Figure 2c) is somewhat similar to that of
275 ozone (Figure 2a), suggesting that differences in $Cl_y+\alpha Br_y$ can explain much of the ozone
276 evolution. However, there is not a simple one-to-one relationship between changes in ozone
277 and those in $Cl_y+\alpha Br_y$. For instance, ozone exceeds 1960s values in the later part of the 21st
278 century, while $Cl_y+\alpha Br_y$ is still above 1960 levels. Also, models with larger values of $Cl_y+\alpha Br_y$
279 (Figure 2c) do not necessarily have larger ozone loss, e.g., MRI and CNRM-ACM have the
280 largest peaks in ozone loss, but do not have the largest changes in $Cl_y+\alpha Br_y$.

281 One possible cause for the lack of a simple relationship between ozone and halogen
282 changes is differences in temperature trends. As shown in Figure 2e, all models show cooling
283 throughout the 21st century, largely from increasing CO_2 concentrations, and this is expected to
284 increase ozone (by slowing down the rate of reactions that destroy ozone). However, it should
285 be noted that over the recent past about 50% of the cooling is associated with the ozone loss from
286 $Cl_y+\alpha Br_y$ [*Shepherd and Jonsson*, 2008]. This cooling explains the increase in ozone above
287 1960 levels before $Cl_y+\alpha Br_y$ returns to 1960 values. Most models cool by about 8-9 K below
288 1960 levels by the end of century, but a few models have cooling exceeding 10 K (CCSRNIES,
289 UMSLIMCAT, LMDZrepro, and CMAM). This is consistent with an expected increase in
290 ozone due to cooling, and these four models have among the largest ozone increases by 2100, as
291 shown in Figure 2b.

292 To quantify the relative contributions of the above mechanisms to ozone changes we now
293 apply an MLR analysis to model outputs. As described in Section 2, the MLR analysis is used to
294 quantify the contributions of changes in $Cl_y+\alpha Br_y$, temperature, NO_y, and HO_x to the ozone
295 changes. As previously discussed in Section 2, there are a number of caveats with this type of
296 analysis and care should be taken in interpreting the results.

297 The contributions from $Cl_y+\alpha Br_y$, temperature, NO_y, and HO_x, are shown in Figures
298 2d,f,h,j, respectively. Differences among models in the contribution from $Cl_y+\alpha Br_y$ are
299 generally similar to relative variations in $Cl_y+\alpha Br_y$ (compare Figures 2d and 2c), with some
300 exceptions. Most notably, MRI and CNRM-ACM have the largest ozone loss at this level from
301 1960-2000 despite not having unusually large amounts of $Cl_y+\alpha Br_y$. This is related to larger
302 sensitivities to $Cl_y+\alpha Br_y$, and we quantify this sensitivity below.

303 Temperature trends play an important role in the return of ozone to above historical
304 levels: the four models with the largest cooling trend (LMDZrepro, CCSRNIES, CMAM, and
305 UMSLIMCAT, see Figure 2e) have the largest increases in ozone relative to 1960 levels (see
306 Figure 2b). The differences in cooling among models explain most of the differences in
307 projected ozone by 2100. Although, again, we note that it is not a simple one-to-one
308 relationship.

309 The contributions from NO_y and HO_x changes are significantly smaller in most cases.
310 Figure 2h,j show the contributions of NO_y and HO_x to ozone changes. For NO_y most models
311 show losses of 0.2-0.3 ppm by 2100 with a few models showing somewhat larger loss, up to a
312 loss of 0.7 ppm in AMTRAC3. While 5 hPa is typically one of the largest loss regions from NO_y
313 changes in volume mixing ratio, HO_x has a much smaller impact at this level and typically is
314 more important at altitudes above 5 hPa [*Jackman et al.,* 1986]. All models show a relatively

315 small contribution (less than 0.1 ppm) from HO_x except ULAQ, which has the largest HO_x trend
316 (see Figure 2i). In general, for the A1b greenhouse gas scenario considered in these CCMVal-2
317 simulations, NO_y and HO_x contributions are much smaller than the contributions from halogen
318 recovery and stratospheric cooling over the 21st century. It is however important to note that this
319 may not be the case for other GHG scenarios [e.g., *Oman et al.*, 2010].

320 The above analysis indicates that changes in $Cl_y+\alpha Br_y$ and temperature dominate tropical
321 ozone evolution at 5 hPa, and differences in the simulated changes in these quantities explain
322 most (but not all) of the variations among the models. To see how representative the changes at
323 5 hPa are over a range of pressures, Figure 3 shows vertical profiles of changes between 2000
324 and 2100 for 25°S-25°N.

325 Figure 3a shows each models reference ozone profile for the year 2000 while changes by
326 2100 appear in Figure 3b. Also, plotted on Figure 3a are Microwave Limb Sounder (MLS)
327 satellite measurements (solid black curve) averaged from 2005-2009. The peak ozone increase is
328 typically at 3 hPa (Figure 3b) with most models centered at around 1.5 ppm. Figure 3c shows
329 that in the upper stratosphere most models have a $Cl_y+\alpha Br_y$ decrease of 2 ppb over this time
330 period. CCSRNIES and SOCOL have larger than average decreases in $Cl_y+\alpha Br_y$ and
331 AMTRAC3 has a smaller than average $Cl_y+\alpha Br_y$ change with a different vertical structure,
332 which is due to how AMTRAC3 treats the breakdown of halogens. Again, we see that MRI and
333 CNRM-ACM have the largest ozone changes due to $Cl_y+\alpha Br_y$ (Figure 3d) with AMTRAC3
334 having the smallest increase over the upper stratosphere. Most models show about equal
335 contributions from decreases in $Cl_y+\alpha Br_y$ and decreases in temperature to the ozone increases
336 over the 21st century. Observations from the MLS [*Santee et al.*, 2008a] for HCl (not shown)

337 suggest that while a few models are in good agreement with MLS in the upper stratosphere,
338 many appear to be on the low end with only CCSRNIES on the high end of observations.

339 Figure 3 shows that the key features seen at 5 hPa hold throughout the upper stratosphere
340 (10 – 1 hPa). Models that have high (low) ozone changes at 5hPa have similar characteristics
341 throughout the upper stratosphere. Also, differences in $Cl_y+\alpha Br_y$ can explain most of the
342 variations among the models with additional contributions from temperature. Figure 3h shows
343 the contribution from NO_y to changes in ozone: it is typically much smaller, and opposite in sign,
344 than changes due to $Cl_y+\alpha Br_y$ or temperature. In general, models show NO_y-related ozone loss
345 of 0.2 ppm around 3-10 hPa, with only AMTRAC3 exhibiting a larger loss. As presented in the
346 Introduction, stratospheric cooling increases NO_y loss [*Rosenfield and Douglass*, 1998] causing a
347 smaller increase (and even some decreases, see Figure 3g) in NO_y over the 21st century than
348 would be expected from N_2O increases in the absence of climate change. The interpretation of
349 changes in lower stratospheric ozone are complicated by the increasingly important impact of
350 transport which is not explicitly included in the MLR analysis and will be discussed in more
351 detail in Section 3.4.

352 As discussed above there are not always one-to-one relationships between changes in
353 $Cl_y+\alpha Br_y$ and temperature and their contribution to ozone changes. One possible reason for this
354 is the different sensitivities of ozone to $Cl_y+\alpha Br_y$ and temperature. Figure 4 shows the vertical
355 profiles of the sensitivity of tropical ozone (25°S-25°N) to $Cl_y+\alpha Br_y$, temperature, and NO_y
356 calculated over the period 1960-2100. Overall there is good agreement between the sensitivities
357 of the various models. All models show a peak $Cl_y+\alpha Br_y$ sensitivity at 3 hPa, mostly around -
358 0.35 ppm/ppb. However, two models stand out with much larger sensitivities, CNRM-ACM (-
359 0.6 ppm/ppb) and MRI (-0.8 ppm/ppb) at 3 hPa.

360 Further insight into the sensitivity of modeled ozone to $Cl_y+\alpha Br_y$ can be gained by
361 examining the abundance of ClO and BrO archived by the various CCMs. Here, we provide a
362 snapshot of the analysis presented in Chapter 6 of *SPARC CCMVal* [2010]. Figure 5 shows
363 profiles of the ClO/Cl_y ratio archived by four of the CCMs at 35°N for Sept 1993 and at 22°N for
364 Feb 1996 (colored lines). The black lines represent the calculated ratio of ClO/Cl_y found using a
365 photochemical steady state (PSS) box model (e.g., *Canty et al.*, 2006 and references therein)
366 constrained by fields of O_3, H_2O, CH_4, Cl_y, NO_y, aerosol surface area, and other constituents
367 archived by each CCM group. Results are shown for four models: the two in question (MRI and
368 CNRM-ACM) and two that archive ClO values that are well explained by the PSS simulation
369 (CMAM and WACCM). The numerical value on each panel is the "metric" assigned to each
370 comparison, with a value of unity indicating perfect agreement with the PSS simulation.

371 The profiles of ClO archived by CMAM and WACCM are in excellent agreement with
372 the PSS simulation, indicating that implementation of the chemical mechanism within these
373 models agrees well with the implementation of the mechanism within the PSS model. However,
374 the MRI ClO profile is much higher (green dashed line, Figure 5) than the profile found using the
375 PSS model. As explained in *SPARC CCMVal* [2010], the MRI chemical mechanism neglected
376 to include the channel for the loss of ClO by the reaction of ClO+OH to yield $HCl+O_2$. This
377 leads to much higher values of ClO than are reported by other models, or observed in the
378 atmosphere [*Santee et al.*, 2008b]. Even when we neglect this reaction channel in our PSS
379 model (black dotted curves, Figure 5), we still can not account for the high values of ClO
380 archived by the MRI group. We conclude the high sensitivity of O_3 to $Cl_y+\alpha Br_y$ exhibited by the
381 MRI model is due to the high concentrations of ClO in this model, due in part to the neglect of
382 the $ClO+OH \rightarrow HCl+O_2$ channel.

383 The reason for the high sensitivity of O_3 to $Cl_y+\alpha Br_y$ within the CNRM-ACM model is
384 not known. For most altitudes, ClO within CNRM-ACM is simulated well by the PSS model.
385 CNRM-ACM does simulate much higher values of ClO just above the tropopause than are
386 accounted for by the PSS simulation; within CNRM-ACM, it appears that chlorine activation is
387 occurring for warmer conditions than suggested by the PSS comparison. The high ClO just
388 above the tropopause can not explain the large sensitivity of O_3 within this model to $Cl_y+\alpha Br_y$
389 shown in Figures 2d, 3d, and 4a. We have examined profiles of BrO within the CNRM-ACM
390 and the PSS model (not shown); we do not believe, based on this comparison, that the high
391 sensitivity of O_3 to halogens exhibited by CNRM-ACM is due to the calculation of BrO within
392 this CCM. It is important to note that the PSS comparisons were done for the REF-B1
393 simulation (1960 to 2000, observed aerosols) whereas the bulk of this analysis is based on the
394 REF-B2 simulation (1960 to 2100, background aerosols). Finally, our comparisons cannot
395 reveal possible errors in the coding of a rate constant that would affect the rate of ozone loss by
396 ClO or BrO, but not affect the abundance of ClO or BrO (i.e., the reaction of ClO+O). The
397 reason for high sensitivity of O_3 to $Cl_y+\alpha Br_y$ within the CNRM-ACM model remains
398 unexplained.

399 We performed an uncertainty analysis of the sensitivities as in *Oman et al.* [2010] and
400 find similar results (not shown). That is, in the mid to upper stratosphere there is relatively more
401 uncertainty in NO_y sensitivity compared to much smaller uncertainty associated with $Cl_y+\alpha Br_y$
402 and temperature.

403 The evolution of upper stratospheric ozone and of the different contributing ozone loss
404 mechanisms at midlatitudes is very similar to that in the tropics (not shown). There are again,
405 reasonably balanced, equal contributions of $Cl_y+\alpha Br_y$ and temperature for the midlatitudes as we

406 found in the tropics. Again MRI and CNRM-ACM stand out with much larger contributions
407 from $Cl_y+\alpha Br_y$ to ozone changes.
408
409 ***3.4 Lower Stratosphere***
410
411 As shown in Figure 1 the evolution of ozone in the tropical lower stratosphere (p > 20
412 hPa) differs from that in the upper portion. This can also be seen in the profiles shown in Figure
413 3b.
414 Although an MLR analysis has been applied to the lower stratosphere, interpretation of
415 these results is complicated by the large role of transport changes and the tight coupling of
416 upwelling and temperature. In the tropical lower stratosphere the loss that the MLR attributes to
417 a temperature change is actually largely a response to increased upwelling, which acts to
418 decrease ozone. This is consistent with *Avallone and Prather* [1996], who showed that changes
419 in upwelling are dominant in controlling tropical lower stratospheric ozone. Temperatures can
420 be reduced by both increased in upwelling and decreased ozone. Previous studies have shown
421 that an increase in the tropical upwelling is the principal cause of a decrease in tropical ozone
422 [*Shepherd,* 2008*; Li et al.,* 2009] with an additional possibly smaller contribution from "reverse
423 self-healing". Reverse self-healing occurs as upper stratospheric ozone rises above historical
424 levels causing less ultra-violet radiation to penetrate into the lower stratosphere resulting in the
425 decreased production of ozone.
426 We examine here the relationship between tropical upwelling and ozone in the CCMVal-
427 2 models. Figure 6 compares the change in tropical ozone (25°S-25°N) at 50 hPa between 1960
428 and 2100 to the corresponding change in the vertical residual velocity (w*) at 70 hpa, for the 12

429 models that provided w* fields. All models show an increase in tropical upwelling and a
430 decrease in ozone over this time period. However, there is a large spread amongst the models in
431 the change in both quantities. There is a fairly compact relationship between these two quantities
432 and a linear fit (black line) nearly intersects the origin indicating that increases in upwelling are
433 the dominant contributor to ozone loss at this level. Most models indicate increases in upwelling
434 of 0.04-0.10 mm/s over this time period and ozone decreases of 0.15-0.35 ppm. SOCOL appears
435 to stand out from this group with significantly larger increases in upwelling and ozone decreases,
436 which act in concert to produce the very large temperature reductions seen in Figure 3e. The
437 impact of this larger change in upwelling in SOCOL can also clearly be seen in both total
438 column ozone change (see Figure 1b), and partial lower stratospheric ozone change (see Figure
439 1h). In general, differences in the change in upwelling explain differences in lower stratosphere
440 tropical ozone in the CCMVal-2 models. Also, this linear relationship exists when using the
441 same level for ozone and w* (both at 50 and 70 hPa).

442 In the midlatitude lower stratosphere transport is also thought to play an important role
443 for ozone changes, which are generally positive over the 21st century, however, the exact role is
444 not quantified in the present analysis (see further discussion below).

445

446 **4. Polar ozone**

447

448 We now consider changes in polar ozone. *Austin et al.* [2010b] evaluate the CCMVal-2
449 model simulations of the Antarctic ozone hole in detail, and describe both the processes that are
450 well simulated and the areas that need additional work. More information on model biases,

451 especially those involving temperature thresholds for PSC formation, are provided in *Austin et*
452 *al.* [2010b].

453 We will first focus on annual average changes and then look at a more detailed analysis
454 of spring when the largest ozone depletion is observed. Figure 7 shows the evolution of annual
455 average southern and northern polar ozone for total column ozone (upper panels, 7a,b), upper
456 partial column (middle, 7c,d) and lower partial column (lower 7e,f). Again, we show ground-
457 based total column ozone measurements (solid black curves, updated from *Fioletov et al.*,
458 [2002]) with respect to 1964 in Figures 7a,b.

459 Evolution of the upper partial columns is very similar to that of midlatitudes (see Figures
460 1d,f). However, the evolutions of the lower and total columns differ. All models show larger
461 peak ozone loss around 2000 in the southern polar region than in the northern polar region. This
462 is expected and seen in observations, as there is greater polar stratospheric cloud (PSC)
463 formation in the southern polar region and a more stable polar vortex that lasts into spring each
464 year. In general there are larger increases in ozone amounts by 2100 compared to 1960 in the
465 northern polar region. It is difficult to say quantitatively with the existing simulations how much
466 of the differences seen by 2100 in the total and partial lower stratospheric column ozone are due
467 to polar chemistry differences, circulation differences, or a combination of the two. Additional
468 simulations with fixed low chlorine concentrations or fixed GHG concentrations could help to
469 quantify the relative impacts.

470 The largest ozone losses occur in the spring in the lower portion of the stratospheric
471 column so we focus on this time and region in more detail. Figure 8a shows the Antarctic (60-
472 90°S) lower stratospheric column ozone for October. Peak ozone loss averages about 100 DU
473 around 2000 with a range from models between 70 and 170 DU. We applied a linear regression

474 analysis to the lower stratospheric column ozone amounts to calculate the contribution from
475 $Cl_y+\alpha Br_y$ using α=60, as appropriate for the polar lower stratosphere.

476 Figure 8b shows the contribution of $Cl_y+\alpha Br_y$ and the residual (Figure 8c), which is much
477 smaller and for most models typically less than ±20 DU. $Cl_y+\alpha Br_y$ dominates the partial column
478 ozone until the end of the 21st century when the residual is in most cases of comparable
479 magnitude. The decrease in mean age of air (i.e. stronger circulation, see Figure 8e) by itself and
480 in combination with upper stratospheric ozone returning to above historical levels acted to cause
481 increased ozone change (i.e, positive residual), however this could be tempered by the cooling of
482 the polar lower stratospheric temperatures (Figure 8f shows 50 hPa temperatures) which occurs
483 in nearly all models.

484 Figure 9a shows the Arctic (60-90°N) lower stratospheric column ozone for March. We
485 also note that this area is typically bigger then the size of the polar vortex so this average also
486 includes mixing effects (also to a lesser extent in the Southern Hemisphere during October).
487 Peak ozone loss averages at 30 DU around 2000 with a range between 10 and 60 DU. Again we
488 linearly regressed the $Cl_y+\alpha Br_y$ against the partial lower stratospheric column ozone. Figure 9b
489 shows the contribution of $Cl_y+\alpha Br_y$ and the residual (Figure 9c), which in this case is generally
490 larger with a consistent 30-40 DU residual by 2100 for most models. This seems to indicate that
491 in the NH polar regions circulation changes cause a larger increase in ozone than seen in the SH
492 by 2100.

493

494 **5. Ozone Recovery**

495

496 The above differences in ozone return dates between regions are summarized in Figure
497 10 which shows the evolution of the multi-model mean (MMM) total and partial column ozone,
498 with respect to 1960 for high latitudes (solid curves) and midlatitudes (dashed curves). Total
499 column ozone for the MMM (Figure 10a) shows a return to 1960 values by the 2030s in the NH
500 in both mid and high latitudes. In the SH the total column ozone MMM exhibits a return to 1960
501 values by the 2060s in the midlatitudes and by 2080 at high latitudes. Nearly all the differences
502 in total column ozone evolution are from the lower portion of the column (500-20 hPa, see
503 Figure 10c) with very similar changes in both hemispheres occurring in the upper portion (Figure
504 10b).

505 Comparing with the evolution of halogens (red curves; using 60-90°S at 50 hPa as a
506 proxy representative value), we see a significant difference in the dates ozone and halogens
507 return to historical levels (i.e., 1960 levels). The MMM Cly+αBry does not return to 1960
508 values by 2100. This is later than the return of ozone (for extratropical regions). The cause of
509 the earlier return of ozone in midlatitudes (shown in Figure 16 in Austin et al., 2010a) in both
510 hemispheres is likely from an increased circulation [*Austin and Wilson*, 2006; *Waugh et al.*,
511 2009; *Li et al.*, 2009] along with increased upper stratospheric ozone from stratospheric cooling.

512 There is a noticeable difference in the dates when northern and southern hemisphere
513 ozone returns to 1960 values (with no such difference in Cly+αBry, not shown). This
514 interhemispheric difference is likely due to interhemispheric differences in transport. Some of
515 the delay in the SH return is likely from asymmetries in polar ozone loss since there is significant
516 polar ozone loss occurring in the SH in the early 21st century when NH ozone is returning to
517 1980 levels (not shown with reference to 1980 levels), causing less ozone to be transported into
518 SH midlatitudes when the vortex breaks down [*Atkinson et al.*, 1989]. The impact of polar ozone

519 losses being transported into the midlatitudes likely play the dominant role in the later return to
520 historical values seen in the SH midlatitudes during first half of the 21st century with any
521 asymmetries in the strengthening of the stratospheric circulation likely having a larger impact
522 toward the later half of the 21st century.
523
524 **6. Conclusions**
525 Simulations of the past and future were preformed using 14 chemistry-climate models for
526 the CCMVal-2 activity. *Austin et al.* [2010a] have examined the evolution of total column ozone
527 and compared the recovery of column ozone and Cl_y in these models. Here we have contrasted
528 the evolution in the upper and lower stratosphere, and examined the cause of the ozone changes
529 (and differences among the models) particularly for the 21st century.
530 The simulations presented here and in *Austin et al.* [2010a] show that there is some
531 general agreement in the ozone evolution among the models, with all showing column ozone
532 decreasing from 1960 to around 2000, and then increasing over the first half of the 21st century.
533 Models also show that the column ozone evolution varies with latitude, especially in the latter
534 half of the 21st century. There are clearly some quantitative differences in ozone evolution
535 across the CCMVal-2 simulations, e.g., a large spread in simulated return of ozone to historical
536 values [*Austin et al.*, 2010a].
537 Separation into partial columns above and below 20 hPa reveals that the latitudinal
538 differences in the evolution of the column ozone are almost completely due to differences in the
539 lower stratosphere (the region of the atmosphere below 20 hPa). In all models, there are only
540 weak latitudinal variations in the evolution of upper stratospheric ozone, and at all latitudes
541 upper stratospheric ozone increases throughout the 21st century and returns to 1960 levels before

542 the end of the century. There is, however, a large spread in dates of return to historical values,
543 with, for example, dates of return to 1960 levels at 5 hPa varying from 2020s to 2060s. A
544 multiple linear regression analysis indicates that the upper stratospheric ozone increase comes
545 from almost equal contributions of decrease in halogens ($Cl_y+\alpha Br_y$) and cooling from increased
546 greenhouse gas concentrations (for the A1b greenhouse gas scenario considered in these
547 simulations), with only small contributions from NO_y and HO_x.

548 In the tropical lower stratosphere there is a steady decrease in ozone through the 21st
549 century in all models, whereas ozone in middle and high latitudes increases during the 21st
550 century. As a consequence tropical column ozone does not return to 1960 levels, whereas
551 extratropical ozone returns or is close to 1960 levels before the end of the century. The decrease
552 of tropical lower stratospheric ozone is due to an increase in tropical upwelling. Models with
553 larger ozone decreases have larger increases in upwelling. Changes in transport also play an
554 important role in the evolution of mid-latitude lower stratospheric ozone, and strongly contribute
555 to the earlier return of ozone than $Cl_y+\alpha Br_y$ to historical values.

556 There are quantitative differences between the hemispheres in the simulated ozone
557 evolution. In particular, ozone returns to historical values earlier in the northern hemisphere. This
558 difference in hemispheric return dates varies between 10 and 50 years depending on the latitude
559 of interest and the reference year (e.g. 1960 or 1980) chosen, and is almost completely related to
560 differences in the lower stratosphere. Additional simulations would need to be completed in
561 order to quantitatively attribute causes for hemispheric differences. However, based on existing
562 simulations it appears that the larger ozone loss from polar chemistry in the SH and the transport
563 of this ozone depleted air into the midlatitudes as the vortex breaks down is one cause, especially

564 during the first half of the 21st century. Changes in the stratospheric circulation could also play a
565 role in these differences.

566 At high latitudes, especially in the SH (Figure 8) $Cl_y+\alpha Br_y$ dominates long-term trends in
567 the lower portion of the column ozone (and total column ozone) with a small (generally positive)
568 residual. This residual is likely caused by circulation changes and upper stratospheric return to
569 above historical levels.

570 These results reinforce the conclusions in *Eyring et al.* [2007] using simulations from the
571 CCMVal-1 activity: decreasing levels of halogens, continued stratospheric cooling, and changes
572 in circulation are the major factors driving 21st century ozone trends. It is important to keep in
573 mind that all of these simulations are based on a single GHG and halogen scenario, with only one
574 model including an interactive ocean. In addition, the use of mixing ratio based halogen
575 boundary conditions rather than emission-based constrains the models response [*Douglass et al.*,
576 2008]. Future work should be done to explore these issues and their impact on ozone evolution
577 in more detail.

578

579 **Acknowledgements**

580 This research was supported by the NASA MAP, ACMAP, and Aura programs and the NSF
581 Large-scale Climate Dynamics program. We would like to thank Susan Strahan for some very
582 helpful comments on this manuscript. We acknowledge the Chemistry-Climate Model
583 Validation (CCMVal) Activity of the WCRP (World Climate Research Programme) SPARC
584 (Stratospheric Processes and their Role in Climate) project for organizing and coordinating the
585 model data analysis activity, and the British Atmospheric Data Centre (BADC) for collecting and
586 archiving the CCMVal model outputs. CCSRNIES research was supported by the Global

587 Environmental Research Fund of the Ministry of the Environment of Japan (A-071) and
588 simulations were completed with the supercomputer at CGER, NIES. The MRI simulation was
589 made with the supercomputer at the National Institute for Environmental Studies, Japan. The
590 contribution from the Met Office Hadley Centre was supported by the
591 Joint DECC and Defra Integrated Climate Programme - DECC/Defra (GA01101). The National
592 Center for Atmospheric Research is operated by the University Corporation for Atmospheric
593 Research under sponsorship of the National Science Foundation. Any opinions, findings, and
594 conclusions or recommendations expressed in the publication are those of the author(s) and do
595 not necessarily reflect the views of the National Science Foundation.
596

596

597 **References**
598
599 Akiyoshi, H., L. B. Zhou, Y. Yamashita, K. Sakamoto, M. Yoshiki, T. Nagashima, M.Takahashi,
600 J. Kurokawa, M. Takigawa, and T. Imamura (2009), A CCM simulation of the breakup of the
601 Antarctic polar vortex in the years 1980-2004 under the CCMVal scenarios, *J. Geophys.*
602 *Res.*, 114, D03103, doi:10.1029/2007JD009261.
603
604 Atkinson, R. J., W. A. Matthews, P. A. Newman, and R. A. Plumb (1989), Evidence of the mid-
605 latitude impact of Antarctic ozone depletion, *Nature* 340, 290-294 (27 July 1989);
606 doi:10.1038/340290a0
607
608 Austin, J., and R. J. Wilson (2006), Ensemble simulations of the decline and recovery of
609 stratospheric ozone. *J. Geophys. Res.*, 111, D16314, doi:10.1029/2005JD006907.
610
611 Austin, J., et al. (2010a), The decline and recovery of total column ozone using a multi-model
612 time series analysis, *J. Geophys. Res.*, Submitted.
613
614 Austin, J., H. Struthers, J. Scinocca, et al. (2010b), Simulations of the Antarctic ozone hole, *J.*
615 *Geophys. Res.*, Submitted.
616
617 Austin, J., and R.J. Wilson (2010c), Sensitivity of polar ozone to sea surface temperatures and
618 halogen amounts, *J. Geophys. Res.*, submitted.
619
620 Avallone L. M., and M. J. Prather (1996), Photochemical evolution of ozone in the lower
621 tropical stratosphere, *J. Geophys. Res.*, 101, 1457-1461.
622
623 Brasseur, G. and M. H. Hitchman (1988), Stratospheric Response to Trace Gas Perturbations:
624 Changes in Ozone and Temperature Distributions. *Science*, 240, 634-367.
625
626 Butchart, N., and A. A. Scaife (2001), Removal of chlorofluorocarbons by increased mass
627 exchange between the stratosphere and troposphere in a changing climate. *Nature* 410,
628 doi:10.1038/35071047.
629
630 Butchart, N., et al. (2006), Simulations of anthropogenic change in the strength of the Brewer-
631 Dobson circulation, *Clim. Dyn.*, 27, 727 741, doi:10.1007/s00382-006-0162-4.
632
633 Canty, T., H. M. Pickett, R. J. Salawitch, K. W. Jucks, W. A. Traub, and J. W. Waters (2006),
634 Stratospheric and mesospheric HOx : Results from Aura MLS and FIRS-2, *Geophys. Res.*
635 *Lett.*, 33, L12802, doi:10.1029/2006GL025964.
636
637 Chipperfield, M. P., and W. Feng (2003), Comment on: "Stratospheric Ozone Depletion at
638 northern mid-latitudes in the 21st century: The importance of future concentrations of
639 greenhouse gases nitrous oxide and methane", *Geophys. Res. Lett., 30*, 1389, doi:
640 10.1029/2002GL016353.
641

642 Daniel, J. S., S. Solomon, R. W. Portmann, R. R. Garcia (1999), Stratospheric ozone destruction:
643 The importance of bromine relative to chlorine. *J. Geophys. Res.*, 104, 23,871-23,880, 598.
644
645 Davies, T, M. J. P. Cullen, A. J. Malcolm, M. H. Mawson, A. Staniforth, A. A. White, and N.
646 Wood (2005), A new dynamical core for the Met Office's global and regional modelling of
647 the atmosphere. *Quart. J Roy. Meteorol. Soc.*, 131, 1759-1782.
648
649 de Grandpre, J., S. R. Beagley, V. I. Fomichev, E. Griffioen, J. C. McConnell, A. S. Medvedev
650 and T. G. Shepherd (2000), Ozone climatology using interactive chemistry: Results from the
651 Canadian Middle Atmosphere Model, *J. Geophys. Res.*, 105, 26,475-26,491.
652
653 Déqué, M. (2007), Frequency of precipitation and temperature extremes over France in
654 ananthropogenic scenario: model results and statistical correction according to observed
655 values. *Global and Planetary Change*, 57, 16-26.
656
657 Douglass, A. R., R. S. Stolarski, M. R. Schoeberl, C. H. Jackman, M. L. Gupta, P. A. Newman,
658 J. E. Nielsen, and E. L. Fleming (2008), Relationship of loss, mean age of air and the
659 distribution of CFCs to stratospheric circulation and implications for atmospheric lifetimes,
660 *J. Geophys. Res.*, 113, D14309, doi:10.1029/2007JD009575.
661
662 Eyring V., N.R.P. Harris, M. Rex, T.G. Shepherd, D.W. Fahey, G.T. Amanatidis, J. Austin, M.P.
663 Chipperfield, M. Dameris, P.M. De F. Forster, A. Gettelman, H.F. Graf, T. Nagashima, P.A.
664 Newman, S. Pawson, M.J. Prather, J.A. Pyle, R.J. Salawitch, B.D. Santer, and D.W. Waugh
665 (2005), A strategy for process-oriented validation of coupled chemistry-climate models.
666 *Bull. Am. Meteorol. Soc.*, 86, 1117–1133.
667
668 Eyring, V., and Coauthors (2006), Assessment of temperature, trace species, and ozone in
669 chemistry-climate model simulations of the recent past. *J. Geophys. Res.*, 111, D22308,
670 doi:10.1029/ 2006JD007327.
671
672 Eyring, V., and Coauthors (2007), Multimodel projections of stratospheric ozone in the 21st
673 century, *J. Geophys. Res.*, 112, D16303, doi:10.1029/ 2006JD008332.
674
675 Eyring, V., A. Gettelman, N. R. P. Harris, S. Pawson, T. G. Shepherd, D. W. Waugh, H.
676 Akiyoshi, N. Butchart, M. P. Chipperfield, M. Dameris, D. W. Fahey, P. M. de F. Forster, P.
677 A. Newman, M. Rex, R. J. Salawitch, and B. D. Santer (2008), Report on the Third SPARC
678 CCMVal Workshop, *SPARC Newsletter No. 30*, p.17-19.
679
680 Fioletov, V. E., G. E. Bodeker, A. J. Miller et al. (2002), Global ozone and zonal total ozone
681 variations estimated from ground-based and satellite measurements: 1964-2000, J. Geophys.
682 Res., 107(D22), 4647, doi:10.1029/2001JD001350.
683
684 Garcia, R. R., D. Marsh, D. E. Kinnison, B. Boville, and F. Sassi (2007), Simulations of secular
685 trends in the middle atmosphere, 1950-2003, *J. Geophys. Res.*, 112, D09301,
686 doi:10.1029/2006JD007485.
687

688 Garcia, R. R., and W. J. Randel (2008), Acceleration of the Brewer-Dobson circulation due to
689 increases in greenhouse gases. *J. Atmos. Sci.*, 65, 2731-2739.
690
691 Grooß, J.-U. and Russell III, J. M. (2005), Technical note: A stratospheric climatology for O_3,
692 H_2O, CH_4, NO_x, HCl and HF derived from HALOE measurements, *Atmos. Chem. Phys.*, 5,
693 2797-2807.
694
695 Haigh, J. D. and J. A. Pyle (1979), A two-dimensional calculation including atmospheric carbon
696 dioxide and stratospheric ozone, *Nature*, 279, 222-224.
697
698 Hegglin, M. I. and T. G. Shepherd (2009), Large climate-induced changes in ultraviolet index
699 and stratosphere-to-troposphere ozone flux, *Nature Geosci.* 2, 687–691.
700
701 IPCC (Intergovernmental Panel on Climate Change) (2000), Special report on emissions
702 scenarios: a special report of Working Group III of the Intergovernmental Panel on Climate
703 Change, 599 pp., Cambridge University Press, Cambridge, U.K.
704
705 IPCC (2001), Third Assessment Report, Working Group I, Intergovernmental Panel on Climate
706 Change, 2001.
707
708 Jackman, C. H., R. S. Stolarski, and J. A. Kaye (1986), Two-dimensional Monthly Average
709 Ozone Balance from Limb Infrared Monitor of the Stratosphere and Stratospheric and
710 Mesospheric Sounder Data, *J. Geophys. Res.*, **91**, 1103-1116.
711
712 Jourdain, L., S. Bekki, F. Lott, and F. Lefevre (2008), The coupled chemistry-climate model
713 LMDz-REPROBUS: description and evaluation of a transient simulation of the period 1980-
714 1999, *Ann. Geophys.*, 26, 6, 1391-1413.
715
716 Lamarque J.-F., D. E. Kinnison, P. G. Hess, and F. M. Vitt (2008), Simulated lower stratospheric
717 trends between 1970 and 2005: Identifying the role of climate and composition changes, J.
718 Geophys. Res., 113, D12301, doi:10.1029/2007JD009277.
719
720 Li, F., R.S. Stolarski, and P.A. Newman (2009), Stratospheric ozone in the post-CFC era, *Atmos.*
721 *Chem. Phys.*, 9, 2207-2213.
722
723 Morgenstern, O., P. Braesicke, F. M. O'Connor, A. C. Bushell, C. E. Johnson, S. M. Osprey, and
724 J. A. Pyle (2009), Evaluation of the new UKCA climate-composition model. Part 1: The
725 stratosphere. *Geosci. Model Dev.*, 1, 43-57.
726
727 Morgenstern, O., and co-authors (2010), A review of CCMVal-2 models and simulations, *J.*
728 *Geophys. Res.* In Press
729
730 Newman, P.A., J.S. Daniel, D.W. Waugh, and E.R. Nash (2007), A new formulation of
731 equivalent effective stratospheric chlorine (EESC), *Atmos. Chem. Phys.*, 7, 4537-4552.
732
733 Oman, L., D.W. Waugh, S.R. Kawa, R.S. Stolarski, A.R. Douglass, and P.A. Newman (2010),

734 Mechanisms and feedbacks causing changes in upper stratospheric ozone in the 21st century,
735 *J. Geophys. Res.*, 114, doi:10.1029/2009JD012397.
736
737 Pawson, S., R. S. Stolarski, A. R. Douglass, P. A. Newman, J. E. Nielsen, S. M. Frith, and M. L.
738 Gupta (2008), Goddard Earth Observing System chemistry-climate model simulations of
739 stratospheric ozone-temperature coupling between 1950 and 2005, *J. Geophys. Res.*, 113,
740 D12103, doi:10.1029/2007JD009511.
741
742 Pitari G., E. Mancini, V. Rizi and D. T. Shindell (2002), Impact of future climate and emission
743 changes on stratospheric aerosols and ozone, *J. Atmos. Sci.*, 59 (3), 414-440.
744
745 Portmann R.W. and S. Solomon (2007), Indirect radiative forcing of the ozone layer during the
746 21st century, *Geophys Res. Lett.*, 34, L02813, doi:10.1029/2006GL028252.
747
748 Randeniya, L. K., P. F. Vohralik, and I. C. Plumb (2002), Stratospheric ozone depletion at
749 northern mid latitudes in the 21st century: The importance of future concentrations of
750 greenhouse gases nitrous oxide and methane, *Geophys. Res. Lett.*, 29 (4), 1051, doi:
751 10.1029/2001GL014295.
752
753 Ravishankara, A. R., J. S. Daniel, and R. W. Portmann (2009), Nitrous Oxide (N_2O): The
754 Dominant Ozone-Depleting Substance Emitted in the 21st Century, *Science*, 326, 123-125.
755
756 Rayner, N. A., D. E. Parker, E. B. Horton, C. K. Folland, L. V. Alexander, D. P. Rowell, E. C.
757 Kent, and A. Kaplan (2003), Global analyses of sea surface temperature, sea ice, and night
758 marine air temperature since the late nineteenth century, *J. Geophys. Res.*, 108(D14), 4407,
759 doi:10.1029/2002JD002670.
760
761 Rind, D., D. Shindell, P. Lonergan, and N. K. Balachandran (1998), Climate change in the
762 middle atmosphere. Part III: the doubled CO2 climate revisited. *J. Clim.* 11, 876-894.
763
764 Rosenfield, J. E., and A.R. Douglass (1998), Doubled CO_2 effects on NO_y in a coupled 2-D
765 model, *Geophys. Res. Lett.* 25, 4381-4384.
766
767 Rosenfield, J. E., A. R. Douglass, and D. B. Considine (2002), The impact of increasing carbon
768 dioxide on ozone recovery, *J. Geophys. Res.*, 107 (D6), 4049, doi:
769 10.1029/2001JD000824.
770
771 Santee, M. L., I. A. MacKenzie, G. L. Manney, M. P. Chipperfield, P. F. Bernath, K. A. Walker,
772 C. D. Boone, L. Froidevaux, N. J. Livesey, and J. W. Waters (2008a), A study of
773 stratospheric chlorine partitioning based on new satellite measurements and modeling, *J.*
774 *Geophys. Res.*, 113, D12307, doi:10.1029/2007JD009057.
775
776 Santee, M. L., et al. (2008b), Validation of the Aura Microwave Limb Sounder ClO
777 measurements, *J. Geophys. Res.*, 113, D15S22, doi:10.1029/2007JD008762.
778
779 Schraner, M., E. Rozanov, C. Schnadt-Poberaj, P. Kenzelmann, A. Fischer, V. Zubov, B. P. Luo,

780 C. Hoyle, T. Egorova, S. Fueglistaler, S. Bronnimann, W. Schmutz, and T. Peter (2008),
781 Technical Note: Chemistry-climate model SOCOL: Version 2.0 with improved transport and
782 chemistry/microphysics schemes. *Atmos. Chem. Phys.*, 8, 5957-5974.
783
784 Scinocca, J. F., N. A. McFarlane, M. Lazare, J. Li and D. Plummer (2008), Technical note: The
785 CCCma third generation AGCM and its extension into the middle atmosphere, *Atmos. Chem.*
786 *Phys,* 8, 7055-7074.
787
788 Shibata, K., and M. Deushi (2008a), Long-term variations and trends in the simulation of the
789 middle atmosphere 1980-2004 by the chemistry-climate model of the Meteorological
790 Research Institute, *Ann. Geophys.*, 26, 1299-1326.
791
792 Shibata, K., and M. Deushi (2008b), Simulation of the stratospheric circulation and ozone during
793 the recent past (1980-2004) with the MRI chemistry-climate model, *CGER's Supercomputer*
794 *Monograph Report Vol.13*, NIES, Japan, 154 pp.
795
796 Shindell, D. T., D. Rind and P. Lonergan (1998), Climate Change and the Middle Atmosphere.
797 Part IV: Ozone Response to Doubled CO_2. *J. Clim, 11*, 895-918.
798
799 Shepherd, T. G. (2008), Dynamics, Stratospheric Ozone, and Climate Change. *Atmos. Ocean*,
800 46, 117-138.
801
802 Shepherd, T. G., and A. I. Jonsson (2008), On the attribution of stratospheric ozone and
803 temperature changes to changes in ozone-depleting substances and well-mixed greenhouse
804 gases, *Atmos. Chem. Phys.*, 8, 1435-1444.
805
806 SPARC CCMVal, SPARC CCMVal Report on the Evaluation of Chemistry-Climate Models, V.
807 Erying, T. G. Shepherd, D. W. Waugh (Eds.), SPARC Report No. 5, WCRP-X, WMO/TD-
808 No. X, http://www.atmosp.physics.utoronto.ca/SPARC, 2010.
809
810 Teyssèdre H., M. Michou, H. L. Clark, B. Josse, F. Karcher, D. Olivié, V.-H. Peuch, D. Saint-
811 Martin, D. Cariolle, J.-L. Attié, P. Nédélec, P. Ricaud, V. Thouret, R. J. van der A, A. Volz-
812 Thomas, and F. Chéroux (2007), A new tropospheric and stratospheric chemistry and
813 transport model MOCAGE-Climat for multi-year studies: Evaluation of the present-day
814 climatology and sensitivity to surface processes, *Atmos. Chem. Phys.*, 7, 5815-5860.
815
816 Tian, W., and M. P. Chipperfield (2005), A new coupled chemistry-climate model for the
817 stratosphere: the importance of coupling for future O3-climate predictions, Quart. J. Roy.
818 Meteorol. Soc., 131, 281-303.
819
820 Tian, W., M.P. Chipperfield, L.J. Gray, and J.M. Zawodny (2006), Quasi-biennial oscillation and
821 tracer distributions in a coupled chemistry-climate model, *J. Geophys. Res.*, 111, D20301,
822 doi:10.1029/2005JD006871.
823
824
825

826 Waugh, D. W., L. Oman, S. R. Kawa, R. S. Stolarski, S. Pawson, A. R. Douglass, P. A.
827 Newman, and J. E. Nielsen (2008), Impact of climate change on stratospheric ozone
828 recovery, *Geophys. Res. Lett.*, *36*, L03805, doi:10.1029/2008GL036223.
829
830 World Meteorological Organization (WMO)/United Nations Environment Programme (UNEP)
831 (2003), Scientific Assessment of Ozone Depletion: 2002, World Meteorological
832 Organization, Global Ozone Research and Monitoring Project, Report No. 47, Geneva,
833 Switzerland.
834
835 World Meteorological Organization (WMO)/United Nations Environment Programme (UNEP)
836 (2007), Scientific Assessment of Ozone Depletion: 2006, World Meteorological
837 Organization, Global Ozone Research and Monitoring Project, Report No. 50, Geneva,
838 Switzerland.
839
840 Yang, E.-S., D. M. Cunnold, R. J. Salawitch, M. P. McCormick, J. Russell III, J. M. Zawodny, S.
841 Oltmans, and M. J. Newchurch (2006), Attribution of recovery in lower-stratospheric ozone,
842 *J. Geophys. Res.*, *111*, D17309, doi:10.1029/2005JD006371.
843
844 Yang, E.-S., D. M. Cunnold, M. J. Newchurch, R. J. Salawitch, M. P. McCormick, J. M. Russell
845 III, J. M. Zawodny, and S. J. Oltmans (2008), First stage of Antarctic ozone recovery, *J.*
846 *Geophys. Res.*, *113*, D20308, doi:10.1029/2007JD009675.
847
848
849
850

850

851 Table 1. Model description and references.

Model	Atmospheric GCM	Domain/Resolution or Truncation	SST/Sea Ice for Ref-B2	Model Reference
AMTRAC3	AM3	Variable, ~200 km, 48 L, 0.017 hPa	CM2.1	Austin and Wilson (2010c)
CAM3.5	CAM	1.9° x 2.5°, 26 L, 3.5 hPa	CCSM3	Lamarque et al. (2008)
CCSRNIES	CCSR/NIES AGCM 5.4g	T42, 34 L, 0.012 hPa	MIROC / IPCC-AR4	Akiyoshi et al (2009)
CMAM	AGCM3	T31, 71 L, 0.00081 hPa	Interactive	Scinocca et al. (2008); deGrandpre et al. (2000)
CNRM-ACM	ARPEGE-Climate version 4.6	T42, 60 L, 0.07 hPa	CNRM-CM3 AR4	Déqué (2007); Teyssèdre et al. (2007)
GEOSCCM	GEOS5	2° x 2.5°, 72 L, 0.015 hPa	HadISST1 for Ref-B1 and CCSM3 for Ref-B2	Pawson et al. (2008)
LMDZrepro	LMDZ	2.5° x 3.75°, 50 L, 0.07 hPa	OPA (ocean), LIM (ice)	Jourdain et al. (2008)
MRI	MJ98	T42, 68 L, 0.01 hPa	MRI-CGCM2.3.2	Shibata and Deushi (2008a,b)
SOCOL	MAECHAM4	T30, 39 L, 0.01 hPa	ECHAM5-MPIOM	Schraner et al. (2008)
ULAQ	ULAQ-GCM	R6/ 11.5° x 22.5°, 26 L, 0.04 hPa	CCSM3	Pitari et al. (2002)
UMSLIMCAT	HadAM3 L64	2.5° x 3.75°, 64 L, 0.01 hPa	HadGEM1	Tian and Chipperfield (2005); Tian et al. (2006)
UMUKCA-METO	HadGEM-A	2.5° x 3.75°, 60 L, 84 km	HadGEM1	Davies et al. (2005); Martin et al. (2006); Morgenstern et al. (2009)
UMUKCA-UCAM	HadGEM-A	2.5° x 3.75°, 60 L, 84 km	HadGEM1	Davies et al. (2005); Martin et al. (2006); Morgenstern et al. (2009)
WACCM	CAM	1.9° x 2.5°, 66 L, 0.00000596 hPa	CCSM3	Garcia et al. (2007)

852 **Figures**

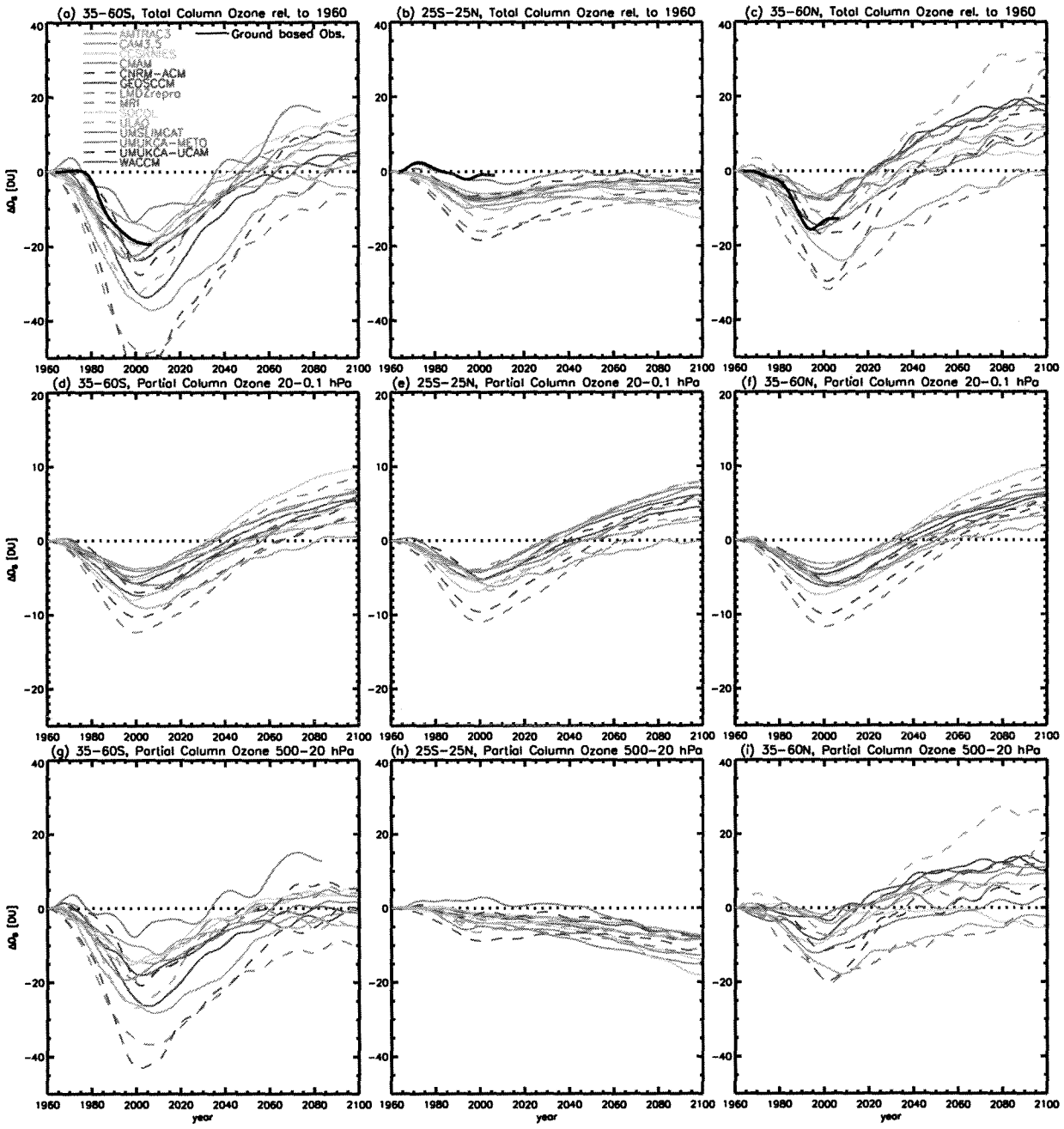

Figure 1. Annual average total and partial column ozone amounts over 3 regions including the tropics (25°S-25°N) and midlatitudes of each hemisphere (35-60°S and °N). The partial column ozone is separated into an upper portion (d,e,f) from 20 to 0.1 hPa and a lower portion (g,h,i) from 500 to 20 hPa. All data are from 1960 to 2100 (except UMUKCA-METO to 2083) and have been smoothed with a 1:2:1 filter iteratively 30 times. Note the scale change in y-axis in panels d,e,f which are half the magnitude of the other panels. Ground-based total column ozone observations (black curves) are shown over 1964-2007 relative to 1964.

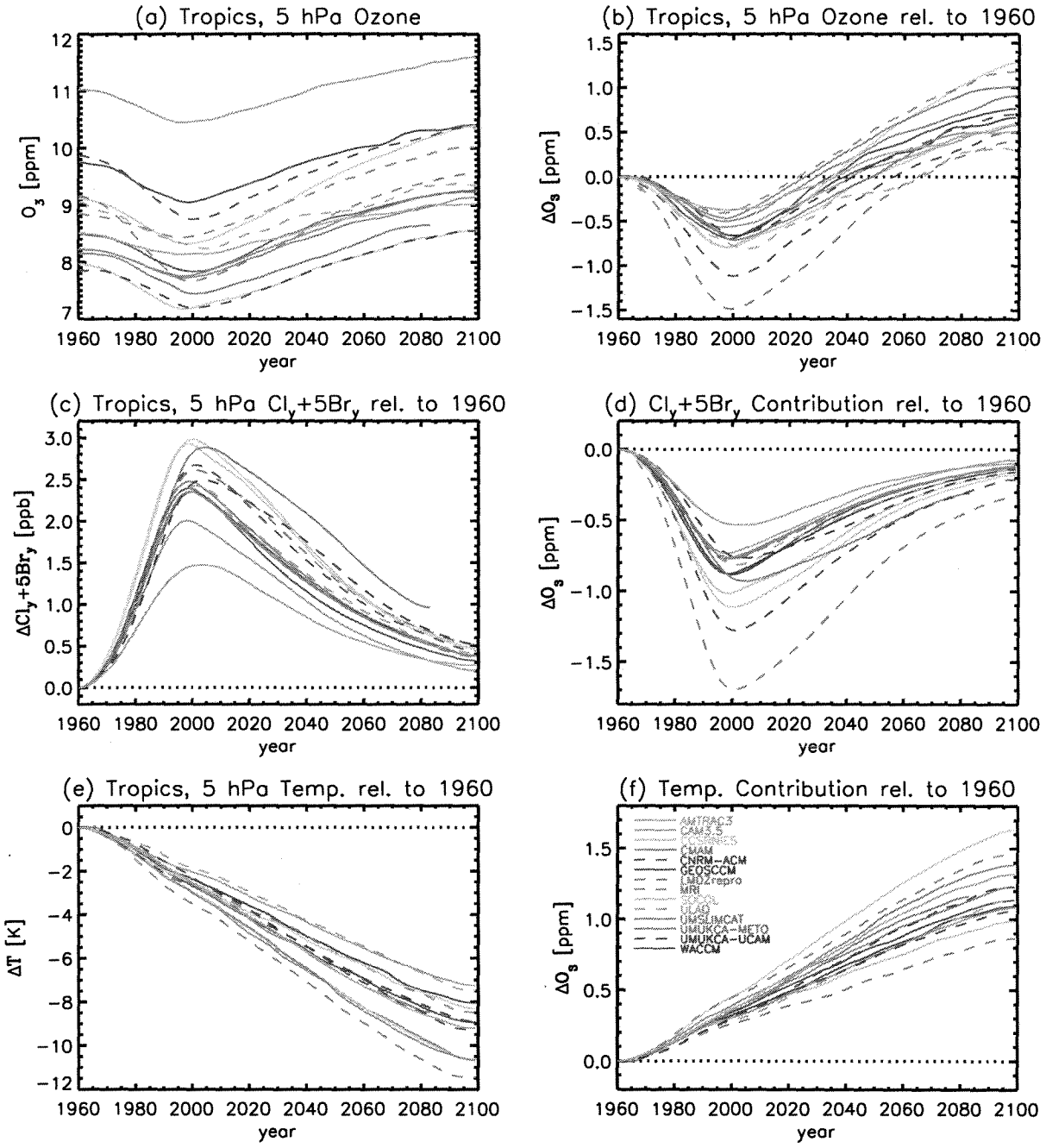

Figure 2. Evolution of ozone (a) in the tropics (25°S-25°N) at 5 hPa and change in ozone (b) with respect to 1960 levels for the CCMVal models. Models change in Cl_y+5Br_y (c) and temperature (e) with respect to 1960 levels. Contribution of changes in Cl_y+5Br_y (d) and temperature (f) to changes in ozone. All models are shown from 1960 to 2100 (except UMUKCA-METO to 2083) and have been smoothed with a 1:2:1 filter iteratively 30 times.

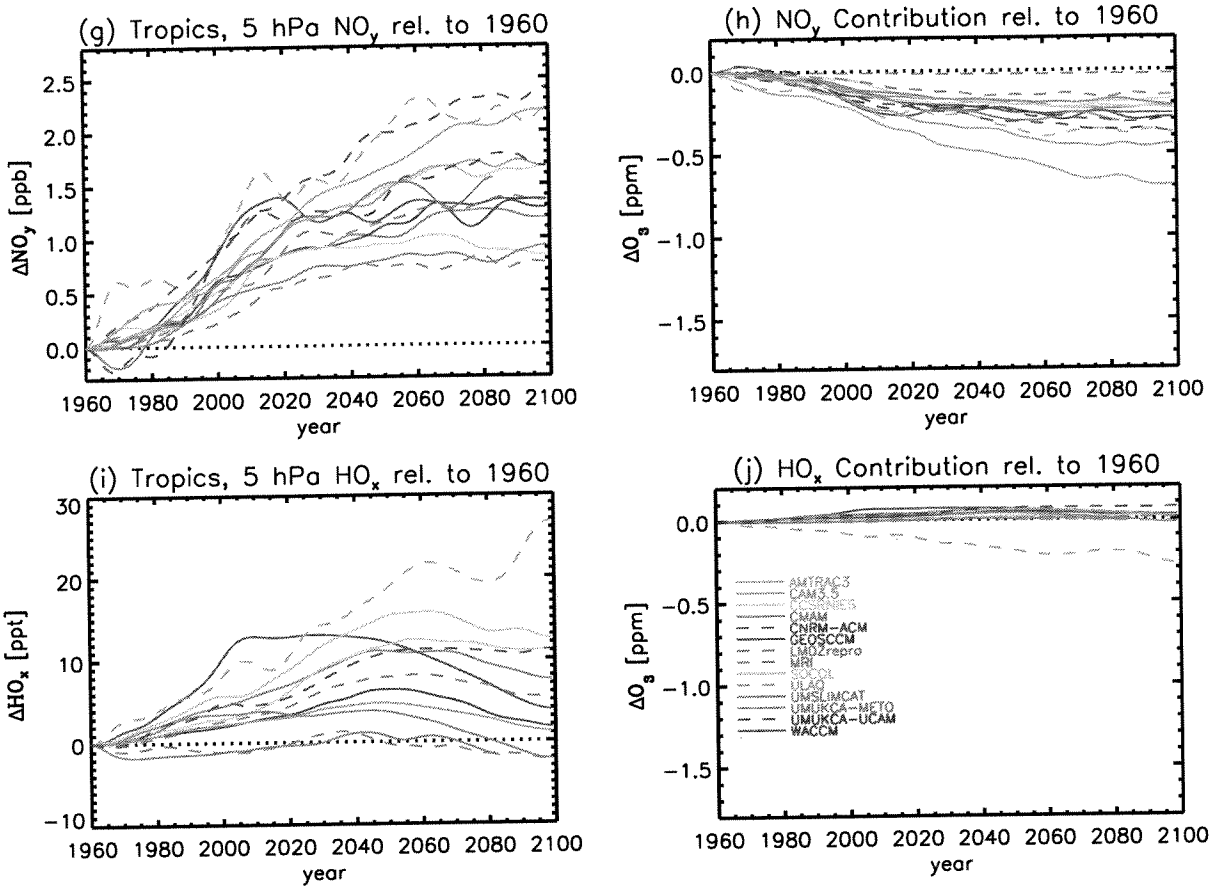

Figure 2 (cont.). Model evolution of NO_y (g) and HO_x (i) with respect to 1960 levels over (25°S-25°N) at 5 hPa. Contribution of changes in NO_y (h) and HO_x (j) to changes in ozone. All models are shown from 1960 to 2100 (except UMUKCA-METO to 2083) and have been smoothed with a 1:2:1 filter iteratively 30 times.

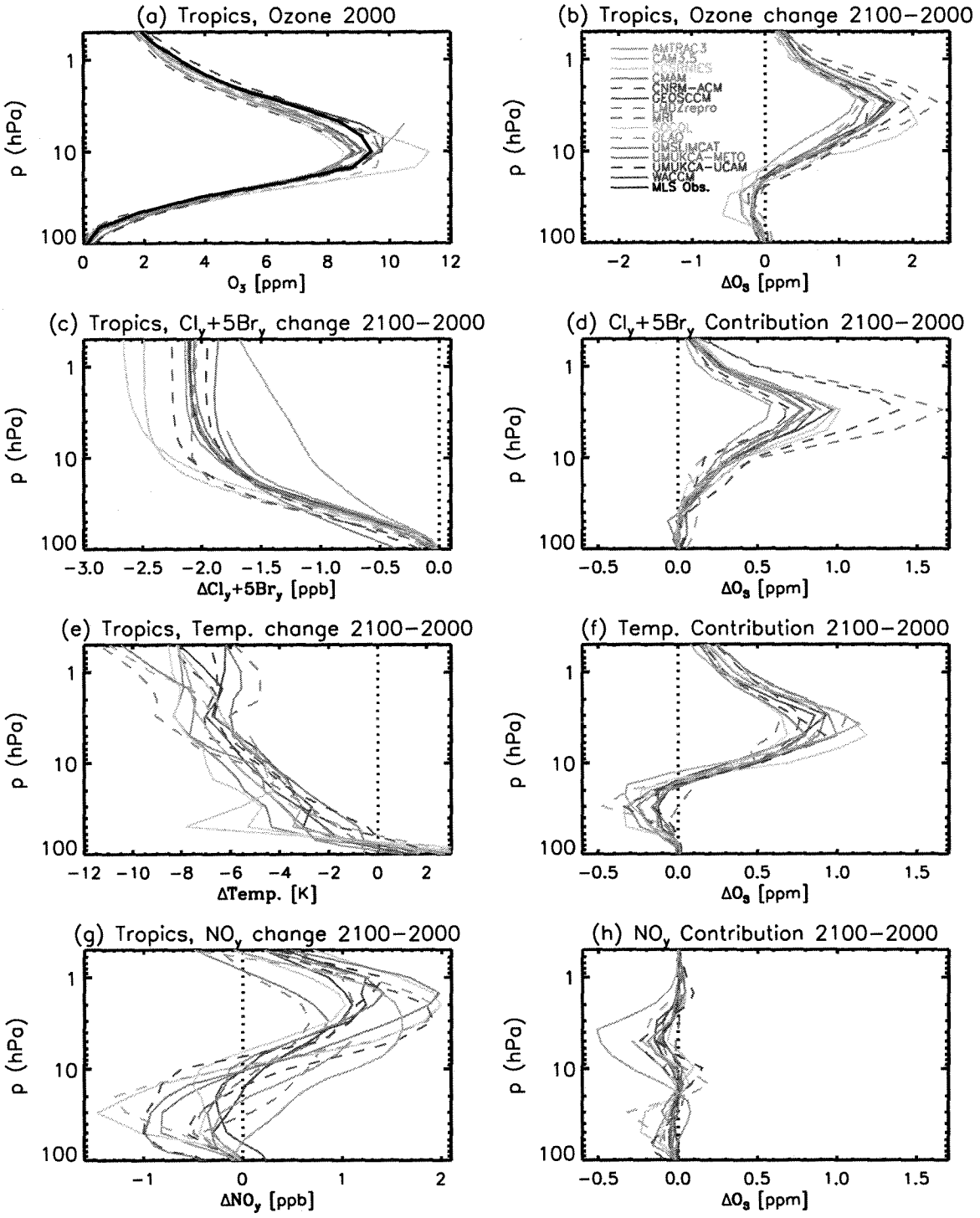

Figure 3. Profiles of ozone (a) in the tropics (25°S-25°N) for 2000 and differences in ozone (b) from 2000-2100 for the CCMVal models. Model differences in Cl_y+5Br_y (c), temperature (e), and NO_y (g) from 2000 to 2100. Also shown are the contributions of changes in Cl_y+5Br_y (d), temperature (f), and NO_y (h) to changes in ozone. Except UMUKCA-METO change shown from 2000 to 2083. Also shown in (a) are observations from MLS (solid black curve) for reference.

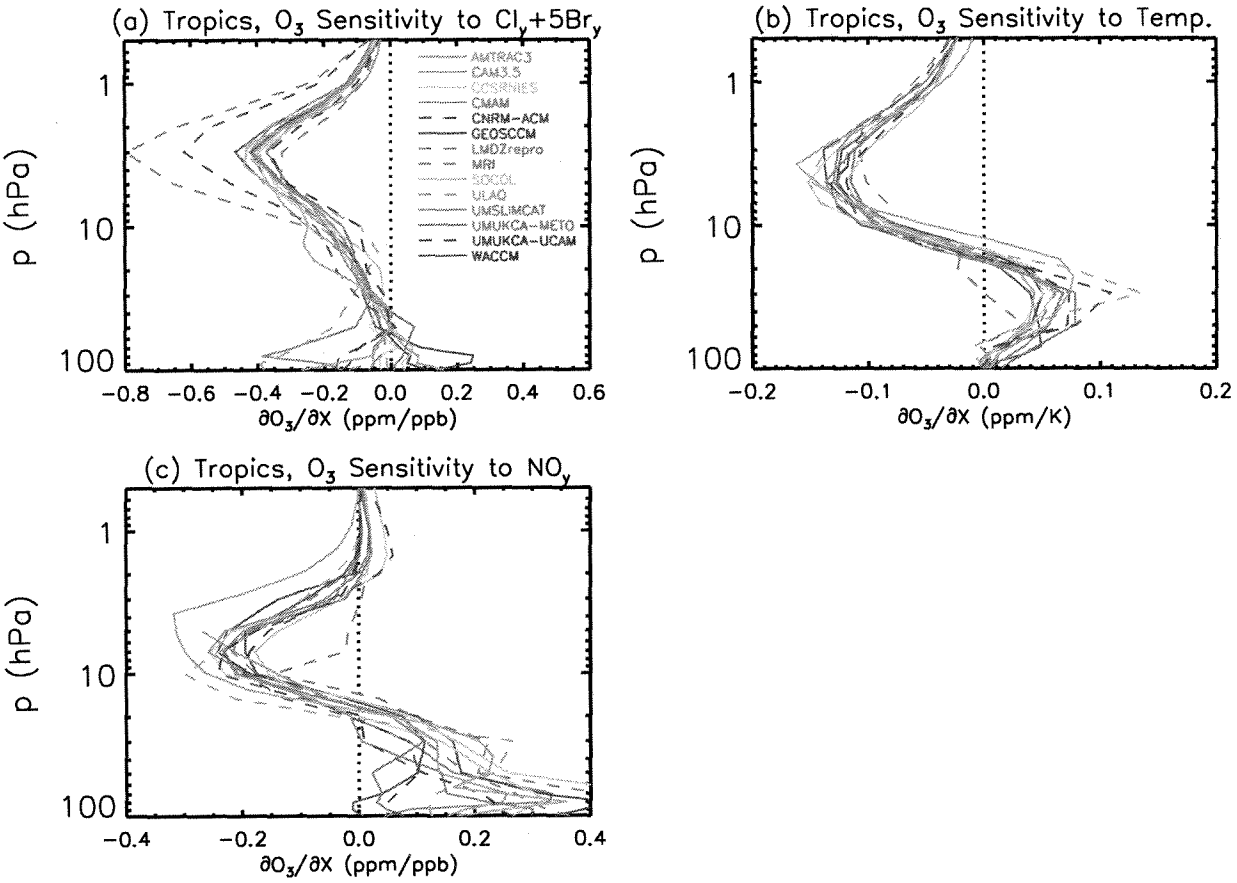

Figure 4. Tropical (25°S-25°N) profiles of the sensitivity of ozone to changes in (a) Cl_y+5Br_y (ppm/ppb), (b) temperature (ppm/K), and (c) NO_y (ppm/ppb).

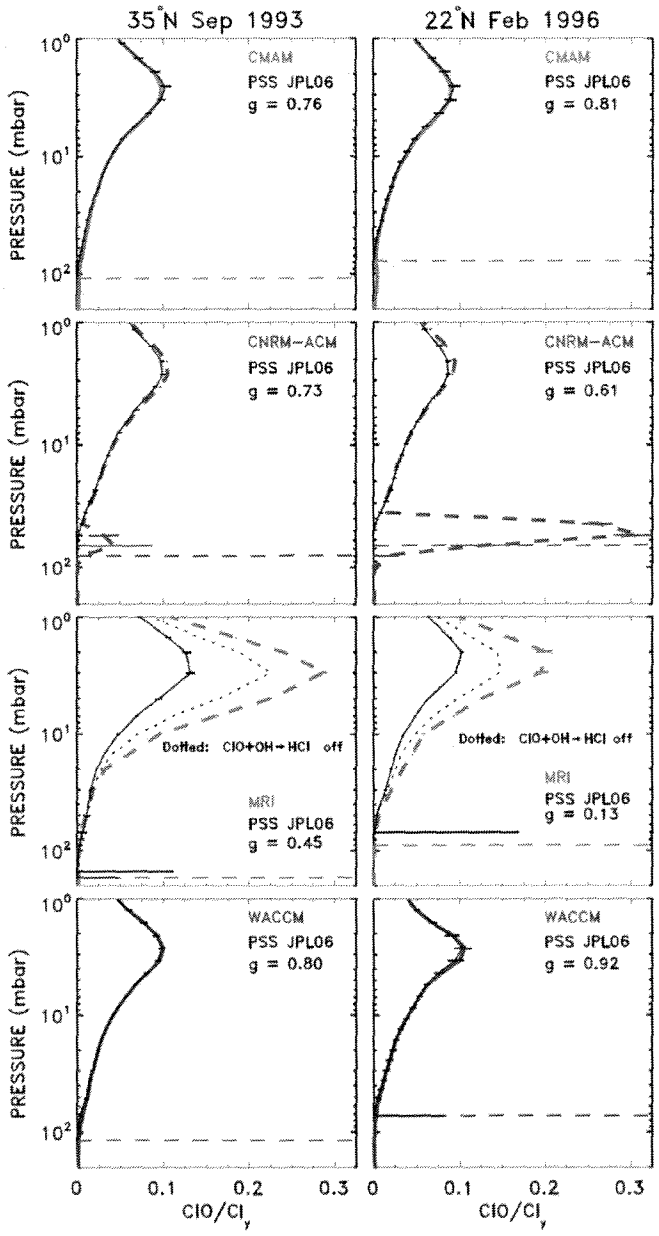

Figure 5. Comparison of zonal, monthly mean profiles of radicals from CCM models (coloured lines) versus 24-hour average radical profiles found using a PSS box model constrained by profiles of T, O_3, H_2O, CH_4, CO, NO_Y, Cl_Y, Br_Y, and sulfate SAD from the various CCMs for the two indicated times and locations. The PSS model was run at CCM model levels from the tropopause (dashed colored lines) to 1 hPa. All simulations used JPL 2006 kinetics. The colored error bars represent the standard deviation about the zonal monthly mean for various days used to compute the mean. The black error bars represent the sensitivity of PSS output to variability in the CCM profiles of radical precursors. The metrics ("values of g") were found as described in Chapter 6 of SPARC CCMVal2 [2010]. For the MRI model, PSS simulations are shown with and without loss of ClO by the reaction $ClO+OH \rightarrow HCl+O_2$.

902

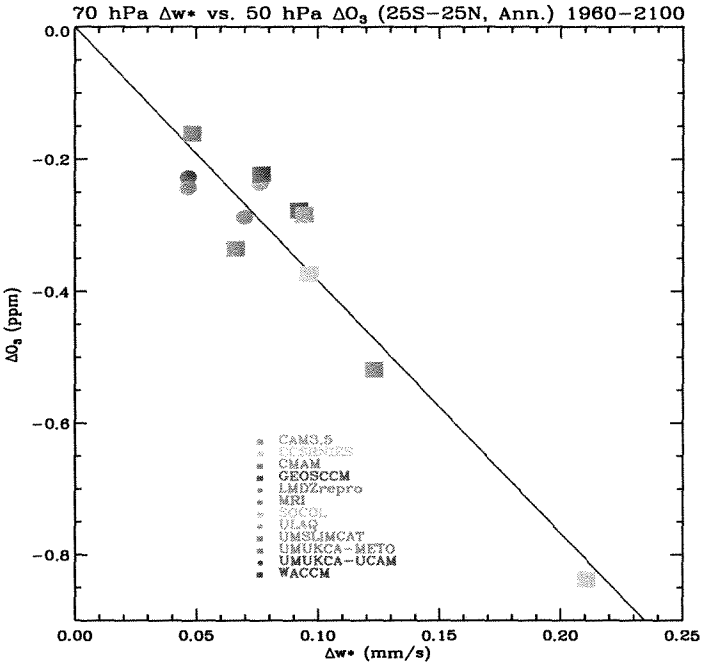

903
904
905
906

907 Figure 6. Scatter plot showing the change (from 1960-2100) in 70 hPa w* and 50 hPa ozone.
908 The values are annual averages over 25°S-25°N for 12 of the CCMVal models with the black
909 line showing the linear fit. UMUKCA-METO change shown from 1960-2083.
910

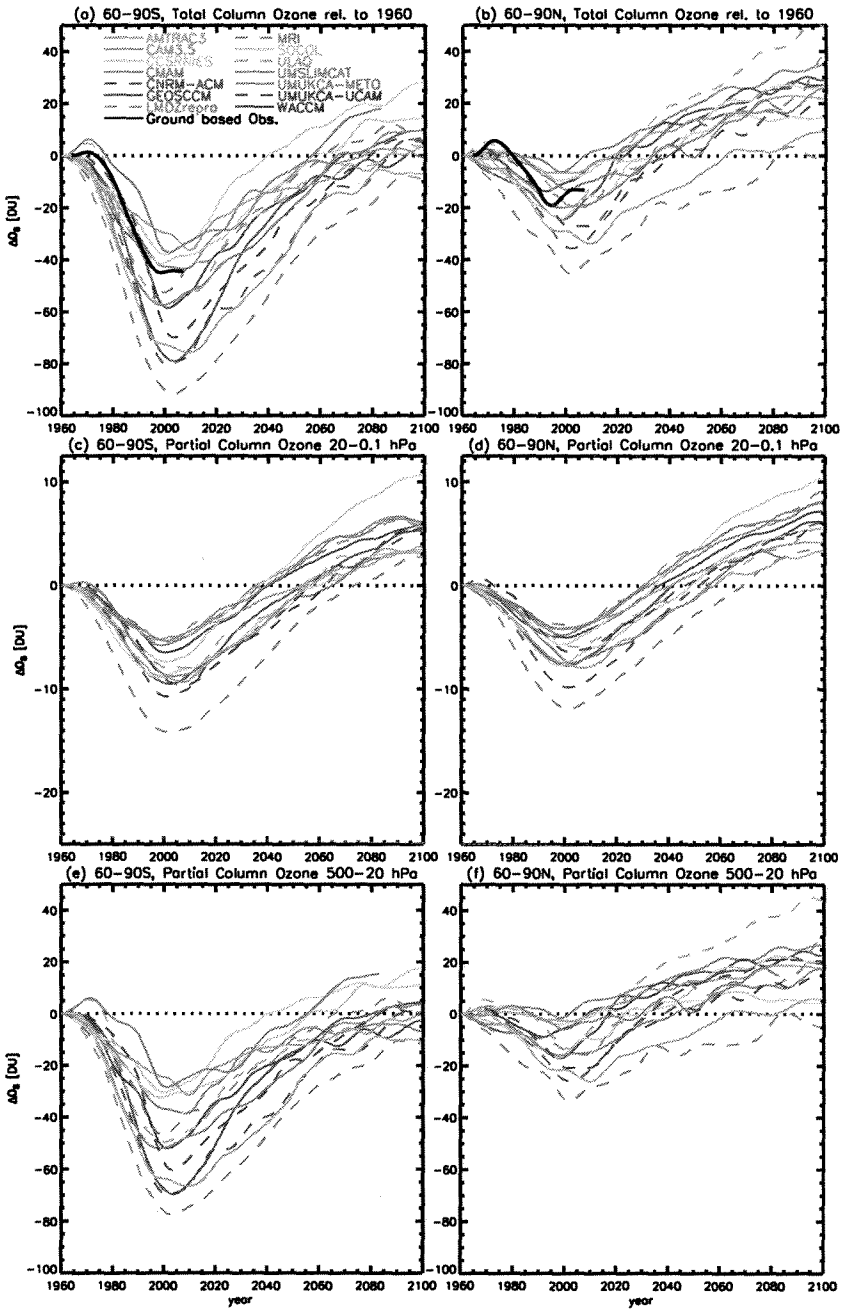

Figure 7. Annual average total and partial column ozone amounts over the high latitudes of each hemisphere (60-90°S and °N). The partial column ozone amounts are separated into an upper portion (c,d) from 20 to 0.1 hPa and a lower portion (e,f) from 500 to 20 hPa. All shown from 1960 to 2100 (except UMUKCA-METO to 2083) and have been smoothed with a 1:2:1 filter iteratively 30 times. Note the scale change in y-axis in c,d. Ground-based total column ozone observations (black curves) are shown from 1964-2007 with respect to 1964.

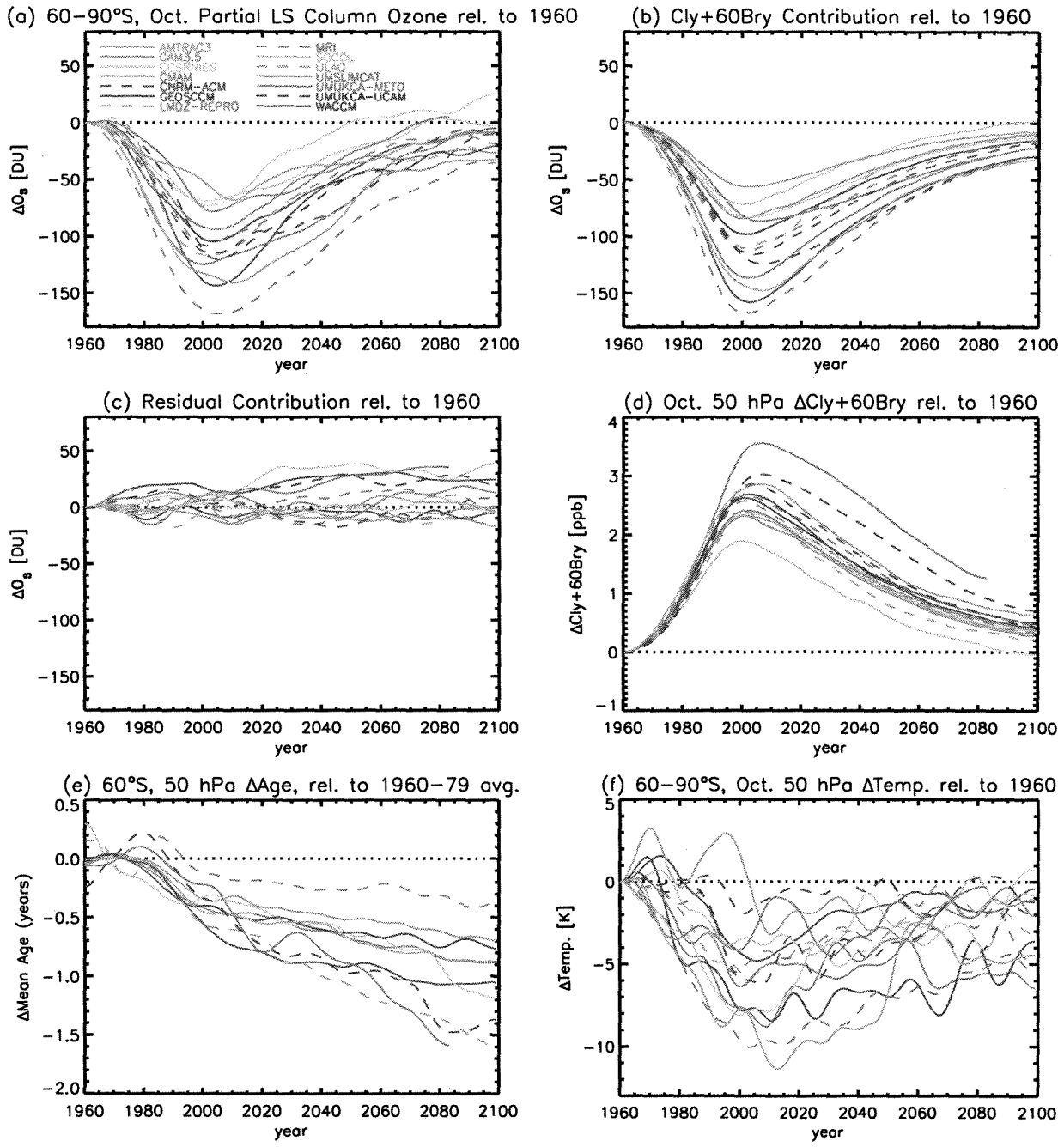

Figure 8. Evolution of ozone (a) for October partial column ozone (500-20 hPa) over 60°-90°S with respect to 1960 levels for the CCMVal models. Model contribution of Cl_y+60Br_y at 50 hPa (b) and residual (c) with respect to 1960 levels. Changes in Cl_y+60Br_y at 50 hPa (d), change in mean age of air (e) for models that included age of air tracer, and (e) change in temperature. All shown from 1960 to 2100 (except UMUKCA-METO to 2083) and have been smoothed with a 1:2:1 filter iteratively 30 times.

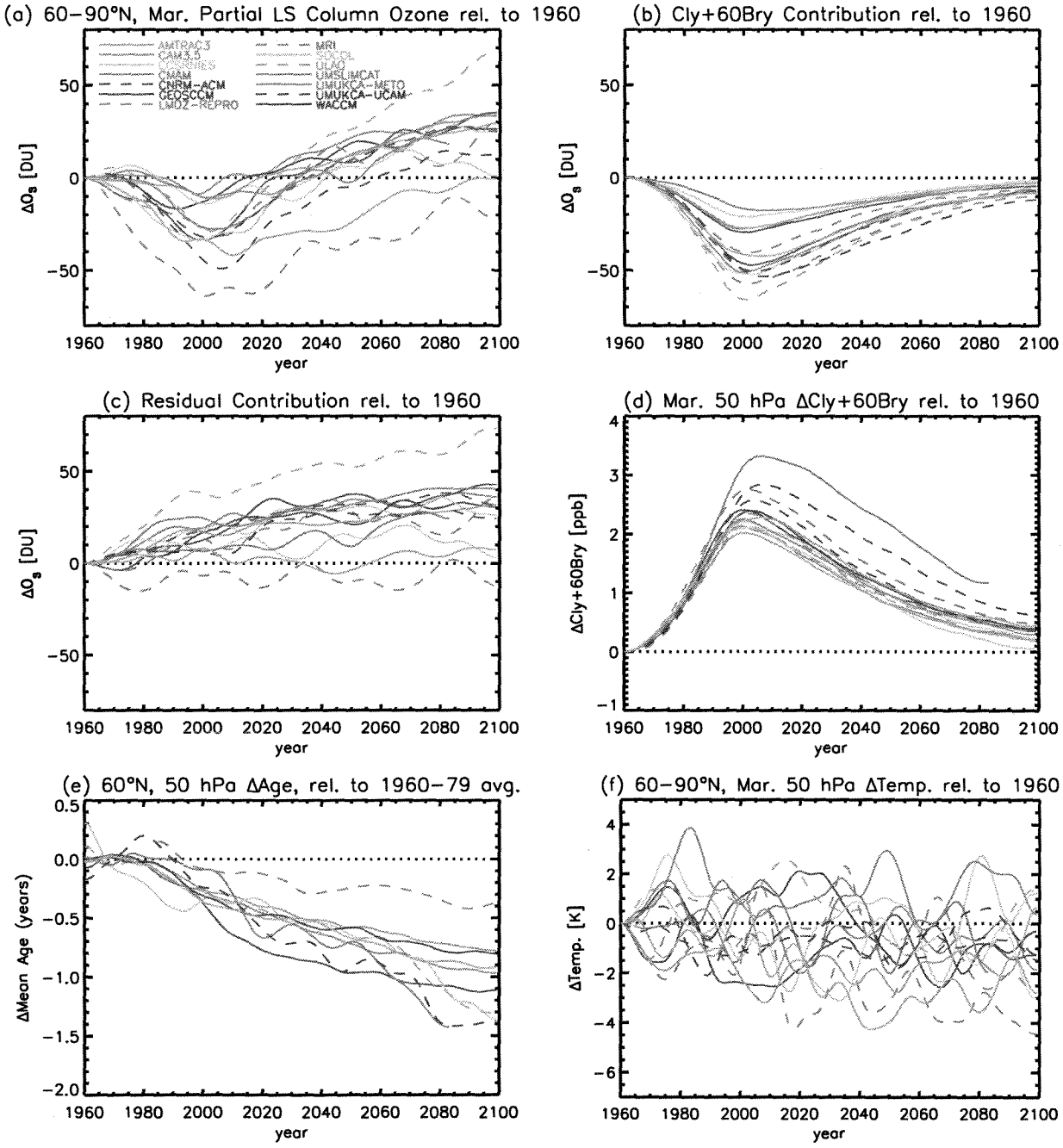

Figure 9. Evolution of ozone (a) for March partial column ozone (500-20 hPa) over 60°-90°N with respect to 1960 levels for the CCMVal models. Model contribution of Cl_y+60Br_y at 50 hPa (b) and residual (c) with respect to 1960 levels. Changes in Cl_y+60Br_y at 50 hPa (d), change in mean age of air (e) for models that included age of air tracer, and change in temperature (f). All shown from 1960 to 2100 (except UMUKCA-METO to 2083) and have been smoothed with a 1:2:1 filter iteratively 30 times.

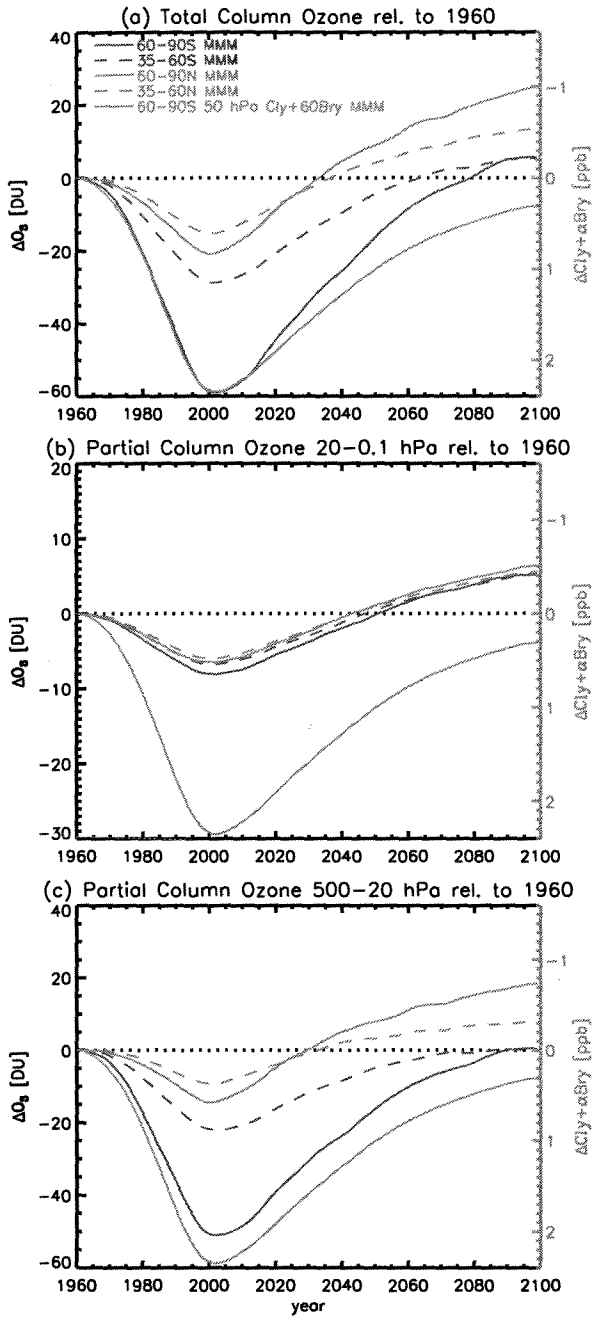

Figure 10. Multi-model mean (MMM) of total (a) and partial column (b,c) ozone amounts for mid (35-60°S and 35-60°N, dashed curves) and high latitudes (60-90°S and 60-90°N, solid curves) and Cly+αBry for high latitudes (60-90°S) for reference.